National Aeronautics and Space Administration

Commercial Satellite Data Acquisition Program

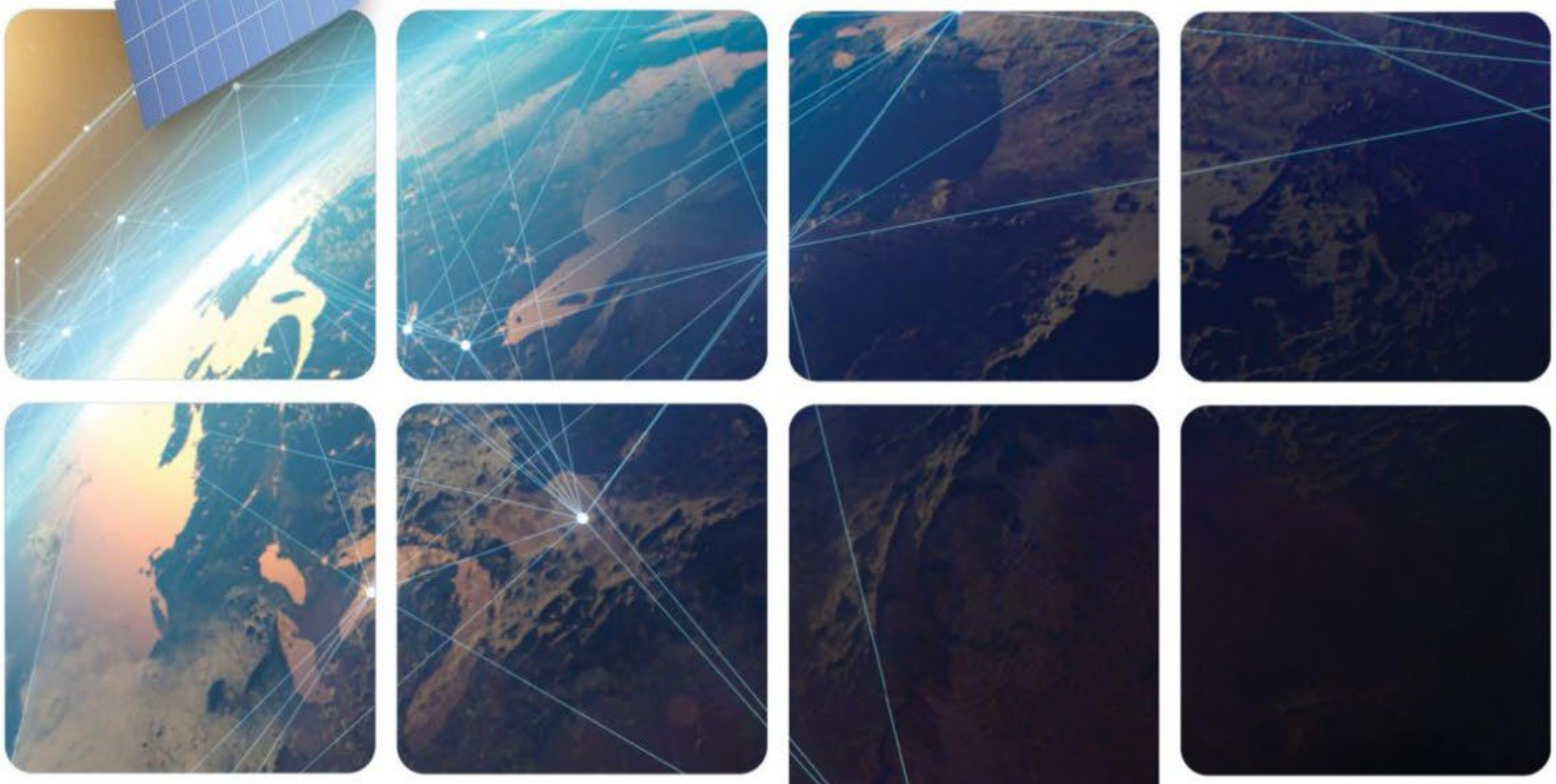

Satellogic NewSat Radiometric & Geometric Quality Assessment Report

Commercial Satellite Data Acquisition Program Satellogic NewSat Radiometric & Geometric Quality Assessment Report

Signature/Approval Page

Approval by:

03/09/2026
Date

Melissa Yang Martin
Commercial Satellite Data Acquisition Program Manager
Earth Science Division
Headquarters/NASA

Accepted by:

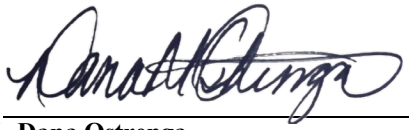

03/09/2026
Date

Dana Ostrenga
Commercial Satellite Data Acquisition Project Manager
Earth Science Division
GSFC/NASA

Preface

This document is under CSDA Project configuration control. Once this document is approved, CSDA approved changes are handled in accordance with Class I and Class II change control requirements described in the CSDA Configuration Management Procedures based on NASA standard configuration practices, and changes to this document shall be made by document change notice (DCN), documented in the Change History Log or by complete revision.

Abstract

The evaluation summarized in this report was conducted by subject matter experts (SMEs) funded by NASA's Commercial Satellite Data Acquisition (CSDA) Program. The SMEs evaluated the radiometric and geometric quality of Satellogic NewSat data for the NASA Earth science research and applications community. The results of the evaluation help to inform NASA program management on the quality of the data for NASA science.

Authored and prepared by

Alana Semple
Science Systems and Applications Inc
National Aeronautics and Space Administration
United States of America

Myungje Choi
University of Maryland, Baltimore Country
National Aeronautics and Space Administration
United States of America

Bin Tan
Science Systems and Applications Inc
National Aeronautics and Space Administration
United States of America

Alexei Lyapustin
Goddard Space Flight Center
National Aeronautics and Space Administration
United States of America

Gary Lin
Goddard Space Flight Center
National Aeronautics and Space Administration
United States of America

Jaime Nickeson
Science Systems and Applications Inc
National Aeronautics and Space Administration
United States of America

Paul Montesano
ADNET Systems Inc
National Aeronautics and Space Administration
United States of America

Frederick Policelli
Goddard Space Flight Center
National Aeronautics and Space Administration
United States of America

Change History Log

Revision	Effective Date	Description of Changes
1.0	03/10/26	First reviewed version for public release

Table of Contents

List of Figures

List of Tables

Acronyms & Abbreviations

AOD	Atmospheric Optical Depth
APA	Absolute Positional Accuracy
AERONET	Aerosol Robotic Network
ATBD	Algorithm Theoretical Basis Document
BBR	Band-to-Band Registration
BRDF	Bidirectional Reflectance Distribution Function
CE90	Circular Error at the 90th percentile
CEOS	Committee on Earth Observation Satellites
CSDA	Commercial Satellite Data Acquisition Program
CWV	Column Water Vapor
DEM	Digital Elevation Model
DESIS	DLR Earth Sensing Imaging Spectrometer
DLR	German Aerospace Center
EO	Earth Observation
EDAP	Earthnet Data Assessment Pilot
ESA	European Space Agency
ESRI	Environmental Systems Research Institute
ESF	Edge Spread Function
FAIR	Findable, Accessible, Interoperable and Reusable
FWHM	Full Width at Half Maximum
GEOTIFF	Geographic Tagged Image File Format
GSD	Ground Sampling Distance
GSFC	Goddard Space Flight Center
L1D	Level 1D
LSF	Line Spread Function
MAIAC	Multi-Angle Implementation of Atmospheric Correction
MDCA	MAIAC Desert Calibration Algorithm
MERRA-2	Modern-Era Retrospective analysis for Research and Applications, Version 2
MODIS	MODerate-resolution Imaging Spectroradiometer
MTF	Modulation Transfer Function
MU	Measurement Unit
NASA	National Aeronautics and Space Administration
NIR	Near Infrared
NIST	National Institute of Standards and Technology
NPL	National Physical Laboratory, UK
PCC	Pearson Cross Correlation
PICS	Pseudo-Invariant Calibration Site
PSF	Point Spread Function
PUG/PUM	Product User Guide/Manual
RadCalNet	Radiometric Calibration Network

RSR	Relative Spectral Response
SBAF	Spectral Band Adjustment Factor
SHARM	Spherical Harmonics radiative transfer code
SME	Subject Matter Expert
SN	NewSat
S-NPP	Suomi-National Polar-orbiting Partnership
SNR	Signal-to-Noise Ratio
SR	Surface Reflectance
SRTM	Shuttle Radar Topography Mission
SSR	Sensor Spatial Response
SZA	Solar Zenith Angle
TCO	Total Column Ozone
TOA	Top-of-atmosphere
VIIRS	Visible Infrared Imaging Radiometer Suite
WV	Worldview sensors (Maxar)

Executive Summary

The Commercial Satellite Data Acquisition (CSDA) Program serves as the central mechanism through which NASA identifies, evaluates, and acquires commercial satellite data in support of its Earth science research and application objectives. These data provide cost-effective opportunities to enhance and complement existing Earth observation capabilities from NASA, other U.S. government agencies, and international partners. This report advances NASA's Earth science mission by contributing to the growing body of CSDA Program documentation on data acquired from the commercial Earth observation sector, specifically, the Satellogic meter-scale NewSat multispectral constellation.

This CSDA Program report focuses on an evaluation of the radiometric and geometric data quality of the NewSat constellation. CSDA acquired NewSat orthorectified top-of-atmosphere (TOA) reflectance products from both satellite generations, Mark IV and Mark V. The Mark IV and V are the most recent instruments comprising their constellation of 44 satellites (as of March 2024). The NewSat satellite constellation was divided into 3 status categories at the start of our assessment, decommissioned, operational and test. We had access to 29 of these, 14 of which were operational and available for tasking, and an archive of both operational and decommissioned sensor data. We tested their tasking system, but tasked just one image, as there was a sufficient archive available to perform our analyses. This evaluation of the NewSat radiometric and geometric performance was carried out by NASA subject matter experts (SMEs) that were enlisted to evaluate the fundamental quality of the Satellogic L1D data products. The guidance used for this assessment followed the joint European Space Agency (ESA)/NASA Optical Mission Quality Assessment Guidelines (ESA-NASA, 2024).

The SME teams requested NewSat data over several evaluation sites submitted by the radiometric and geometric evaluation teams. The CSDA program acquired 60 orthorectified TOA reflectance products, referred to as Level 1D (L1D), across 7 evaluation sites, resulting in data from 17 different NewSat satellites during the period of 2021-2025. The evaluation report is divided into two parts, a Data Provider Documentation Review section and a Detailed Validation section. The first part includes 3 sections, product details, metrology, and product generation, where the information provided here was gathered from product documentation provided. The detailed validation section is divided into two parts, each including an evaluation of multiple metrics defining radiometric and geometric quality.

The radiometric quality assessment team used the Libya 4 pseudo-invariant calibration site (PICS) to perform their analysis. Libya 4 is part of a set of reference test sites defined by the Committee on Earth Observation Satellites (CEOS). The radiometric performance metrics evaluated include radiometric calibration, signal-to-noise ratio (SNR) and the temporal stability. The calibration was assessed relative to the MODerate-resolution Imaging Spectroradiometer (MODIS) sensor aboard the Aqua satellite. This assessment found that the NewSat NIR bands had the largest differences from the spectral reference, overestimating radiance across all scenes collected from 4 of the satellites sampled. Of the 16 bands in this 4-sensor sample (each with 4 bands), 11 had gains within 10% of the reference data. There were 9 out of the 16 bands with SNRs above 100, resulting in a

grade of ‘Good’. Overall, the Mark V satellite analyzed exhibited more consistent gain and SNR values in the RGB bands compared to the Mark IV satellites. No noticeable trends were found in a temporal stability assessment of top-of-atmosphere reflectance across time series ranging from 6-weeks to 1-year from the 4 satellites examined. Due to the low number of samples available a robust assessment of temporal stability across a time series was not possible.

The geometric assessment team uses spatial validation sites such as the Baotou, China calibration and validation test site along with additional scenes acquired over several spatially distinct features such as those within cities. The geometric performance metrics included sensor spatial response (SSR), absolute positional accuracy, band-to-band registration and temporal stability. The two generations of Satellogic sensors behaved differently from a geometric perspective and thus were graded separately. The geometric validation section is where the differences between Mark IV and Mark V generations of the NewSat sensors were most apparent. In particular, the sensor spatial response analysis had the most surprising results. Both generations were found to have a lower spatial resolution than specified in the documentation, with averages of 1.4 m for Mark IV, specified at 1 m, and 2.1 m for Mark V, specified at 0.7 m. We found with both generations, the NIR band had a consistently lower spatial resolution than the visible bands. The absolute positional accuracy (the sensor Circular Error at the 90th percentile, or CE90) was assessed at 17.4 m (~18 pixels) and 17.0 m (~24 pixels) for Mark IV and Mark V satellites, respectively. The geometric temporal stability (at CE90) results indicated 9.7 m (10 pixels) and 9.3 m (~13 pixels), for Mark IV and Mark V satellites, respectively, although within specification, these variations may not allow for detailed time-series analyses. The band-to-band registration of the data are within specification, where geolocation offsets between bands improve from Mark IV (0.4 m) to Mark V (0.32 m). These results suggest that this geometric characteristic is reliable for many scientific use cases.

Based on these radiometric and geometric validation results we recommend Satellogic Mark IV and Mark V data be made available for NASA scientific use, depending on specific science objectives and use cases.

Note: *As of the time of publication, Satellogic has changed aspects of their data processing, in part to address issues reported here. CSDA is engaged in a quality assessment of their revised products and will report on the results in the near future.*

1 Background

The Commercial Satellite Data Acquisition (CSDA) Program was established by NASA’s Earth Science Division (ESD) in 2020 following the successful completion of the Private-Sector Small Constellation Satellite Data Product Pilot. The program’s primary objective is to identify, evaluate, and acquire commercial remote sensing data that enhances NASA’s Earth science research and applications. CSDA provides structured on-ramping opportunities for emerging commercial satellite data vendors, enabling NASA to continuously integrate innovative data sources as the private sector evolves. By leveraging these partnerships, NASA’s ESD aims to accelerate scientific discovery and expand applications of Earth observation data for societal benefit.

Since the initial pilot, the Program has conducted three on-ramp activities, resulting in the addition

of several vendors into sustainment. In 2024, CSDA streamlined its evaluation process by introducing high-quality, SME-led data assessments, accelerating reviews and strengthening NASA's engagement with the rapidly growing commercial data ecosystem. This evaluation framework not only ensures NASA gains timely access to high-quality, mission-relevant commercial data, but also provides valuable feedback to private-sector providers, fostering innovation, improved data products, and alignment of industry capabilities with NASA's evolving scientific needs.

1.1 Satellogic NewSat Constellation Evaluation

The Satellogic Mark IV and Mark V satellites provide very high-resolution commercial multispectral imagery in 4 spectral bands Blue, Green, Red, and Near-infrared (NIR), with a minimum daily revisit interval. Some of the characteristics of the constellation are captured in Table 1 below.

Table 1. Characteristics of the Satellogic NewSat constellation.

Satellogic MSI Constellation & Capabilities						
	Initial Launch	Pixel Size	Bands	Satellites	Swath	Revisit
Mark IV	Jan 2020	0.99 m	4 VNIR	22	5 km	Subdaily
Mark V	Apr 2022	0.7 m	4 VNIR	7	6.5 km	Subdaily

Satellogic Products
Raw (L0)
L1 Basic (L1B
Ortho ready (L1C)
Ortho (L1D)

Tasking	
Available at 4 priority levels	
Min AOI	50 sq km
Max AOI	500 sq km

Note that the satellites listed here include both active and decommissioned sensors that we had access to from the Satellogic archive.

This evaluation assessed both the radiometric and geometric performance of both the Satellogic Mark IV and Mark V imagery across a total of 7 sites (Figure 1) specific to each team. Overall, the SME teams acquired 60 Satellogic NewSat TOA reflectance product (L1D ortho) images from 17 different NewSat satellites collected between 2021-2025. The radiometric quality assessment team used 24 images, from 4 different NewSat sensors, collected over the Libya 4 pseudo-invariant calibration site to analyze 3 metrics of radiometry, radiometric calibration, signal-to-noise ratio (SNR), and temporal stability. The geometric quality assessment team used 36 images, acquired from 16 different NewSat sensors, from the 6 sites indicated in Figure 1. The Baotou calibration and validation site in China, which features a large high-contrast checkerboard pattern, was used to assess the NewSat sensor spatial response (SSR). The team also requested imagery from multiple urban areas with spatially distinct features useful for evaluating geometric fidelity. The geometric evaluation focused on SSR, absolute positional accuracy, band-to-band registration, and temporal stability using both NewSat satellite generations. Figure 1 below shows the locations of the radiometric and geometric sites used in this quality assessment report.

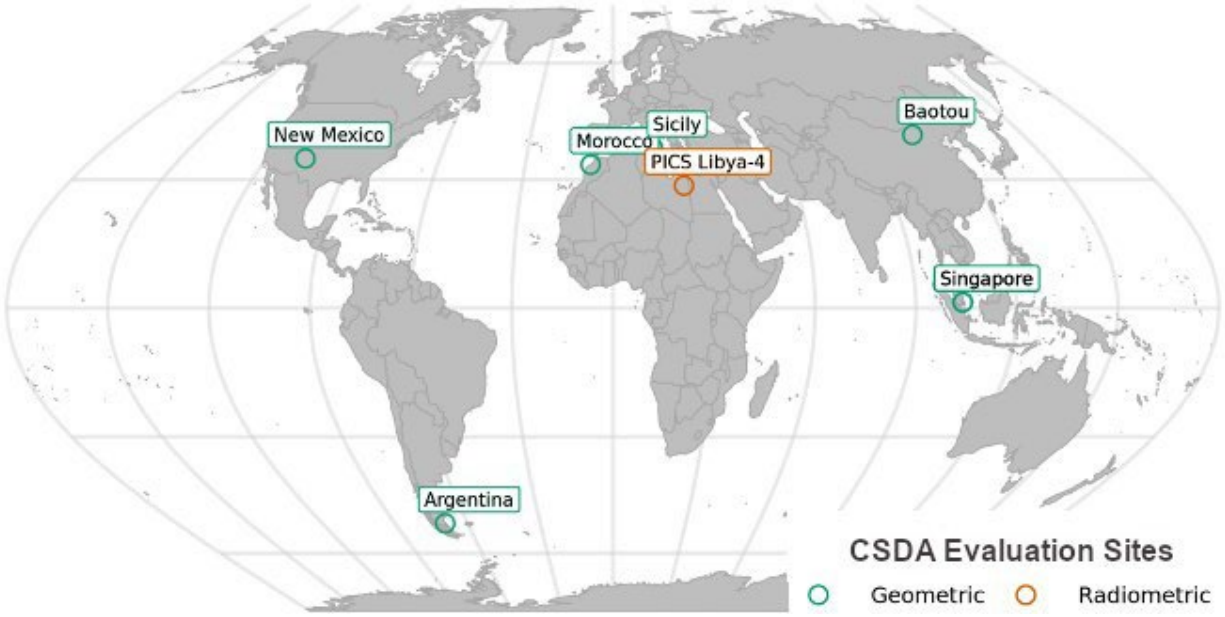

Figure 1. Overview map of the site locations used for the evaluation of Satellogic Mark IV and Mark V imagery.

2 Validation Maturity Matrices

2.1 Summary Maturity Matrix

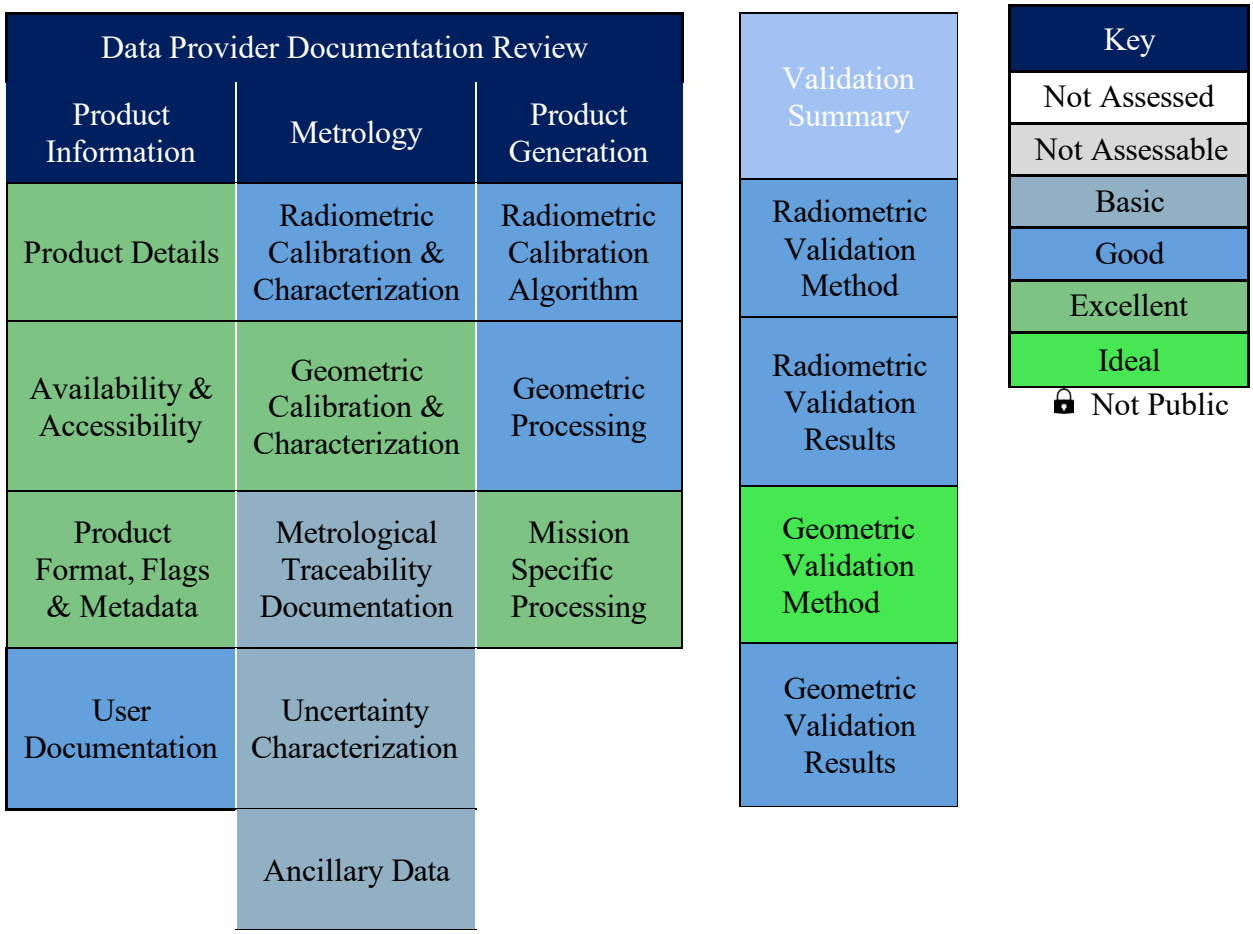

Figure 2. Summary Maturity Matrix for Satellogic NewSat L1D product.

2.2 Detailed Validation Maturity Matrix

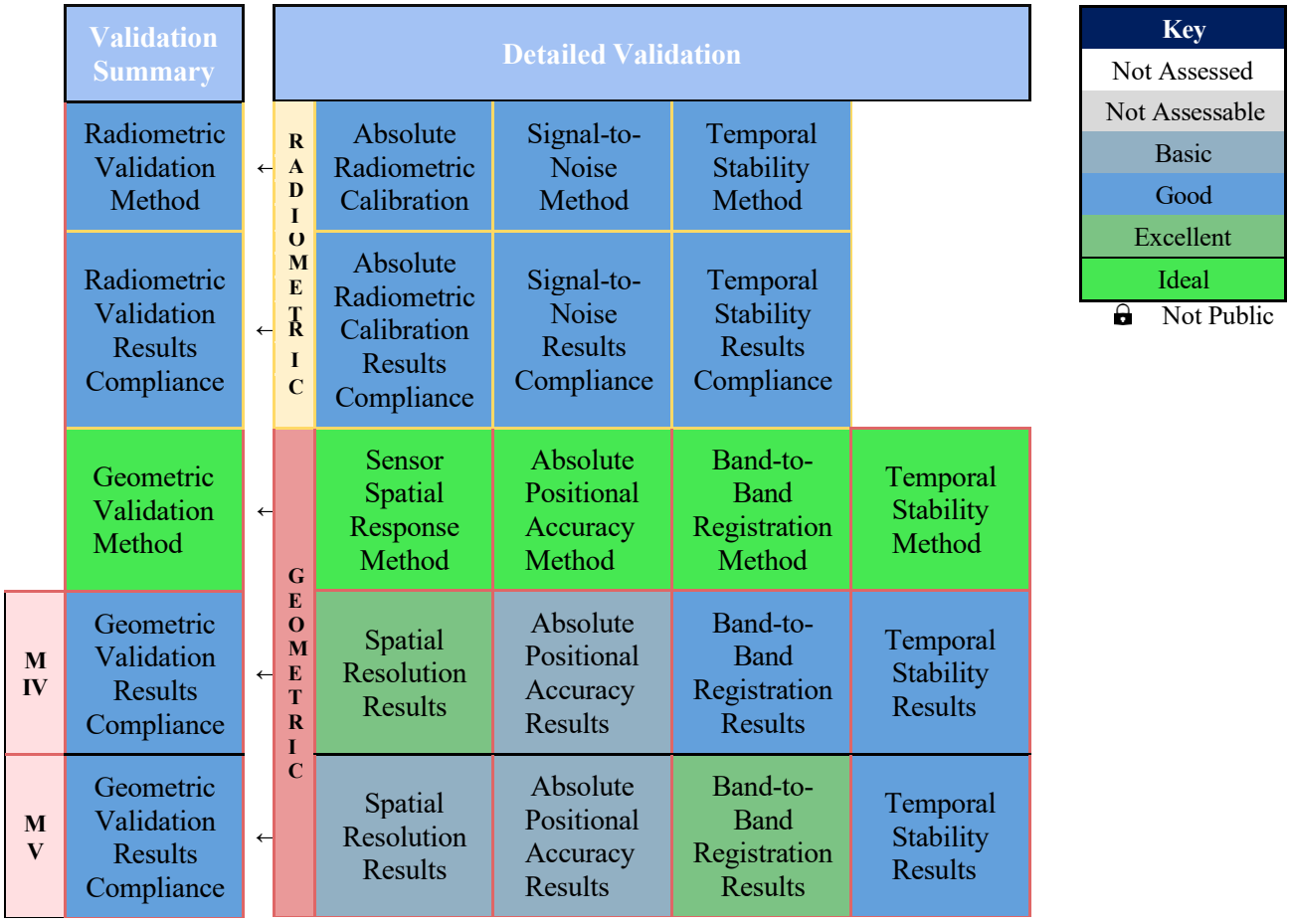

Figure 3. Detailed Validation Maturity Matrix for the optical domain, including the Validation Summary column from the Summary Validation Maturity Matrix.

3 Data Provider Documentation Review

3.1 Product Information

Product Details	
Grade: Excellent	
Justification	*The Satellogic product details were all available within the online documentation.*
Product Name	*L1D Basic*
Sensor Name	*NewSat Mark IV and Mark V*
Sensor Type	*Multispectral camera - 4-bands (B,G,R,NIR)*
Mission Type	*29-satellite Constellation, active and decommissioned, 22 Mark IV, 7 Mark V (as of Jan 2025)*
Mission Orbit	*Sun Synchronous, high inclination*
Product Version Number	*1.1.2*
Product ID	*{DATE}_{TIME}_{SECOND_DECIMALS}_{PAYLOAD}_{SATELLITE}_{PRODUCT}_{VERSION}_{SUFFIX}.{EXTENSION}* ● *DATE: Year(4 digits)month(2 digits)day(2 digits)* ● *TIME: Hour(2 digits)minute(2 digits)second(2 digits)* ● *SECOND_DECIMALS: All the decimal part from the timestamp seconds* ● *PAYLOAD: MS for multispectral (4 bands)* ● *SATELLITE: Satellite name* ● *PRODUCT: i.e., L1C* ● *VERSION:* ● *SUFFIX: depends on the asset, might be RPC, or nothing for example.*
Processing level of product	*Level 1*
Measured Quantity Name	*16-bit TOA reflectance*
Measured Quantity Units	*unitless*
Stated Measurement Quality	*Satellogic has a desired spec of <10% error*
Spatial Resolution	*Mark IV 0.99 m, Mark V 0.70 m, GSD*
Spatial Coverage	*5 km swath (Mark IV), 6.5 km (Mark V), collection strips can be 2000 km in length for Mark IV and up to 9000 km for Mark V.*
Temporal Resolution	*5 orbits/day at equator, 15 at the poles*
Temporal Coverage	*Daily*

Point of Contact	*Taylor Struzik (taylor.struzik@satellogic.com)* *Gonzalo Castillo (gon@satellogic.com)*
Product locator (DOI/URL)	
Conditions for access and use	*U.S. Government, End-User License Agreement (USG EULA)*
Limitations on public access	*Yes*
Product Abstract	

Availability & Accessibility	
Grade: Excellent	
Justification	*The data are easily accessible and meet most of FAIR principles.*
Compliant with FAIR principles	*85%*
Data Management Plan	*Yes*
Availability Status	*Available. Data can be accessed via Aleph. Aleph is Satellogic's unified platform for discovering, purchasing, and managing satellite imagery.*

Product Format, Flags & Metadata	
Grade: Excellent	
Justification	*The data are provided in GeoTIFF format, accompanied by several metadata files. Pixel-level cloud mask information was also included. For each processing level, metadata components are described in tabular form, with clear presentation of variable names, descriptions, and examples. Variable naming adheres to community standards.*
Product File Format	*GeoTIFF*
Metadata Conventions	*STAC, ISO 19115-2*
Analysis Ready Data?	*No*

User Documentation	
Grade: Good	
Justification	*Product information is available, accessible via the online documentation. However, there is no dedicated ATBD. Some non-standard metadata are described in the documentation but not included in the delivered metadata*
Document	***Reference***
Product User Guide	*https://developers.satellogic.com/imagery-products/introduction.html*
ATBD	*Not available*

3.2 Metrology

Radiometric Calibration & Characterisation	
Grade: Good	
Justification	*Each component of pre-launch radiometric calibration and characterization, on-orbit calibration, and vicarious calibration are documented. Absolute calibration relies on vicarious calibration with Sentinel-2 over several RadCalNet sites. Components for converting from digital number to top-of-atmosphere radiance/reflectance (e.g., Gain factor, vicarious calibration factor, solar irradiance) are provided with SI units in the metadata. However, the uncertainty budget associated with each method is not addressed, making it difficult to assess whether all aspects of sensor behavior have been fully considered.*
References	• https://developers.satellogic.com/imagery-products/introduction.html

Geometric Calibration & Characterisation	
Grade: Excellent	
Justification	*Pre-launch tests are performed but not disclosed. Geometric post-launch tests have been performed and disclosed in a proprietary document.*
References	• *Proprietary*

Metrological Traceability Documentation	
Grade: Basic	
Justification	*While a basic traceability chain across processing levels (L0 to L1D) is provided, level-specific traceability details and an uncertainty propagation diagram are both absent.*
References	• https://developers.satellogic.com/imagery-products/l0.html

Uncertainty Characterisation	
Grade: Basic	
Justification	*The overall radiometric uncertainty of TOA reflectance is provided based on intercomparison with Sentinel-2; however, sensor-specific or scene-specific uncertainties are not available. The sources of uncertainty are also not described. Known limitations are qualitatively listed, but no corresponding indicators are included in the metadata.*
References	• https://developers.satellogic.com/imagery-products/msi_payload_specifications.html • https://developers.satellogic.com/imagery-products/image_processing.html

Ancillary Data	
Grade: Basic	
Justification	*Some ancillary data (e.g., DEM, solar model, an ESRI image map) are used in the processing, with sources partially disclosed. For example, the source of the solar model is provided, whereas the source of the DEM is not specified.*
References	• https://developers.satellogic.com/imagery-products/image_processing.html#frame-to-gcps-matching • https://developers.satellogic.com/imagery-products/image_processing.html#top-of-atmopshere-reflectance-correction • https://www.arcgis.com/home/item.html?id=10df2279f9684e4a9f6a7f08febac2a9 • https://www.nrel.gov/grid/solar-resource/spectra-astm-e490

3.3 Product Generation

Radiometric Calibration Algorithm	
Grade: Good	
Justification	*Reasonable radiometric calibration algorithms are applied across various processing stages, including pre-launch lab measurements and on-orbit vicarious calibration. Several components, such as bad pixel filtering, global correction, and vicarious calibration, are described in sufficient detail. However, a few processes (e.g., straylight correction) are only briefly described.*
References	https://developers.satellogic.com/imagery-products/image_processing.html

Geometric Processing	
Grade: Good	
Justification	*Most geometric processing is described in satisfactory detail. However, the reference digital elevation model (DEM) used is not specified.*
References	• https://developers.satellogic.com/imagery-products/image_processing.html

Mission-Specific Processing	
Grade: Excellent	
Cloud mask	
Justification	*All cloud mask processing is documented in an open access github repository with scientific publications and accuracy assessment. Cloud mask values are clearly explained.*
Reference	• https://developers.satellogic.com/imagery-products/l1basic.html • https://github.com/dlr-eoc/ukis-csmask

4 Detailed Validation – Radiometric

4.1 Absolute Calibration

4.1.1 Method

We performed a radiometric validation to examine both the long-term calibration stability and a vicarious calibration relative to the Moderate-Resolution Imaging Spectroradiometer (MODIS) sensor aboard the Aqua satellite platform. A pseudo-invariant calibration site (PICS), Libya 4 (28.55°N, 23.39°E), located in the Sahara Desert, was used for radiometric calibration and evaluation because it does not exhibit strong seasonal or annual changes in reflectance. In general, PICS are recommended by CEOS for use in sensor calibration, and the Libya 4 site is recognized for its high radiometric stability, low aerosol levels, and large homogeneous area (https://calval.cr.usgs.gov/apps/libya-4). Figure 4 illustrates these characteristics based on images from the Mark V sensor NewSat-41.

The Multi-Angle Implementation of Atmospheric Correction (MAIAC) team at NASA Goddard Space Flight Center (GSFC) applied the MAIAC Desert Calibration Algorithm (MDCA) to assess long-term calibration stability and to facilitate cross-sensor calibration relative to Aqua MODIS, used here as the radiometric calibration reference sensor. This approach has been used for the vicarious calibration of several satellite sensors, including MODIS aboard Terra [Lyapustin et al., 2014], the Visible Infrared Imaging Radiometer Suite (VIIRS) aboard the Suomi-National Polar-orbiting Partnership (S-NPP) platform, NOAA-20, and NOAA-21 [Lyapustin et al., 2023], and the Maxar constellation [Choi et al., 2024].

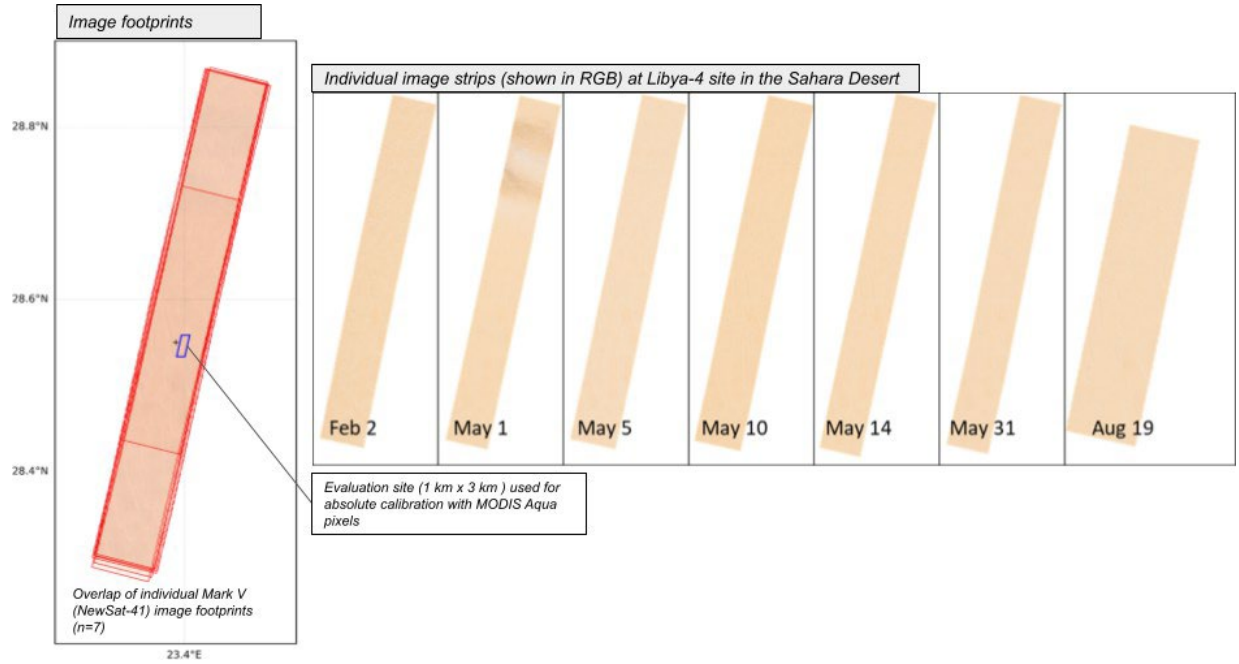

Figure 4. Satellogic NewSat-41 (Mark V) images over Libya 4 in 2024 exhibit high radiometric stability, low aerosol levels, and high spatial homogeneity across all scenes. The blue box at the left denotes the 1×3 km² area selected for absolute calibration evaluation with Aqua MODIS, and the red boundaries indicate the footprints of the individual observations.

For the radiometric calibration evaluation, we used the Satellogic Level 1D (L1D) "Ortho" product from the NewSat sensors across both Mark IV and V generations. This product is described as radiometrically corrected, orthorectified, and map-projected imagery suitable for both scientific and commercial applications. According to the data provider, identical radiometric corrections are applied across Level 1B ("Basic"), Level 1C ("Ortho Ready"), and Level 1D ("Ortho") products. The Satellogic NewSat L1D data includes top-of-atmosphere (TOA) reflectance in the Blue, Green, Red, and NIR bands, along with metadata providing the conversion factor for TOA radiance.

We collected L1D imagery over the Libya 4 site from 4 NewSat satellites: 3 Mark IV satellites (NewSat-10, -27, and -31) and 1 Mark V satellite (NewSat-41). These satellites were selected because each had 5 or more images over the Libya 4 site (24 total images), allowing for meaningful statistical analysis. A list of the images used in the analysis is summarized in Appendix Table A1. As the Mark V satellites are the newer generation, at the time of data purchase, only one NewSat sensor was able to provide the minimum of 5 images over the site.

We standardized the radiometric comparisons of the NewSat data to a reference of Aqua MODIS data for the evaluation. We did this by accounting for differences in sensor measurement characteristics, such as relative spectral response functions, observation time, and viewing geometry. The MDCA enables the simulation of TOA reflectance either at the actual measurement date/time and viewing geometry or under a normalized geometry, defined by a fixed solar zenith angle (e.g., 20°) and nadir view (i.e., view zenith angle of 0°). This was achieved using aerosol optical depth (AOD), column water vapor (CWV), and surface bidirectional reflectance distribution function (BRDF) derived from MODIS MAIAC processing collocated with each NewSat image. Due to the daily global coverage of MODIS, the majority of the NewSat observations can be spatially and temporally collocated with corresponding MODIS MAIAC retrievals. In addition, total column ozone (TCO) concentrations from the Modern-Era Retrospective analysis for Research and Applications, Version 2 (MERRA-2) reanalysis were incorporated. With these atmospheric and surface inputs, the NewSat TOA radiance and reflectance were simulated using the Spherical Harmonics (SHARM) radiative transfer code [Lyapustin, 2005]. The resulting simulated TOA radiance provides a reference for evaluating the absolute radiometric calibration of the Satellogic NewSat satellites and assessing their long-term temporal consistency. The overall MDCA workflow is illustrated below in Figure 5.

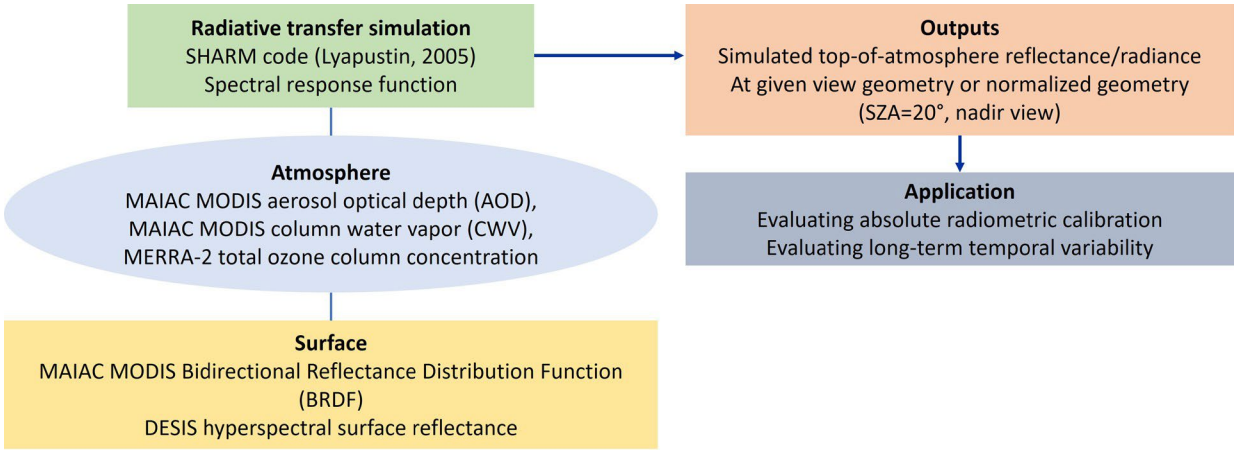

Figure 5. Schematic diagram of radiometric validation using MAIAC desert calibration algorithm (MDCA).

We focused on a 1×3 km² area near the center of the Libya 4 region, consisting of three adjacent 1×1 km² MODIS sinusoidal grid cells (Figure 6). This area was chosen for its relatively low spatial variability, reducing the influence of prominent sand dune ridges and valleys. NewSat measurements were then spatially aggregated into the three MODIS grid cells using an area-weighted average, which helps to mitigate residual spatial heterogeneity caused by small-scale sand dune features and enables collocation with the ancillary products.

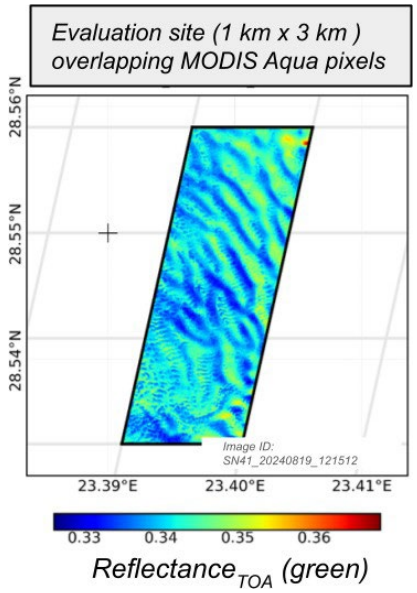

Figure 6. The top-of-atmosphere reflectance in the green band observed by NewSat (SN)-41 on August 19, 2024, at 12:15:12 UTC shows the relative homogeneity typical of this site. Three 1×1 km² MODIS sinusoidal grid cells (grey) that overlap with this image provide reference reflectance. The plus marker ('+') indicates the center location of Libya 4 site.

To account for spectral differences between the Aqua MODIS and Satellogic NewSat sensors, we derived Spectral Band Adjustment Factors (SBAFs) for surface reflectance (SR) using hyperspectral data from the German Aerospace Center's (DLR's) Earth Sensing Imaging Spectrometer (DESIS) instrument aboard the International Space Station (ISS). Since 2018, DESIS has been capturing Earth's reflected spectral radiance across the 400–1000 nm range, with a spectral sampling interval of 2.55 nm and a spectral resolution of approximately 3.5 nm [Krutz et al., 2019; Alonso et al., 2019]. DESIS collects data for 235 spectral channels, and offers a spatial resolution of 30 m, with 1024 across-track pixels and a swath width of about 30 km. Our previous analysis indicates strong radiometric consistency between DESIS and Aqua MODIS [Lyapustin et al., 2023].

The DESIS hyperspectral SR data was spectrally convolved with the relative spectral response (RSR) functions of the MODIS and NewSat sensors. The convolved surface reflectance ($\rho\rho_{ccccccccccccccccc}$) is calculated using the following equation:

$$\rho\rho_{ccccccccccccccccc} = \frac{\sum \rho\rho_{\lambda\lambda} EE_{\lambda\lambda} RRRRRR_{\lambda\lambda ccdd}}{\sum EE_{\lambda\lambda} RRRRRR_{\lambda\lambda ccdd}},$$

where $\rho\rho_{dd}$ is DESIS SR, EE_{dd} is solar irradiance, and $RRRRRR_{dd}$ is the spectral response function. The ratio of the convolved SR values for MODIS and NewSat over the Libya 4 site yields the SBAFs used to spectrally adjust the MODIS BRDF, enabling simulation of NewSat TOA radiance or

reflectance. Figure 7 illustrates the spectral convolution process using DESIS data and the computation of SBAFs.

Figure 8 presents the convolved SR values in all four bands for both MODIS and NewSat. The final SBAF is obtained by averaging individual SBAF values from six different DESIS measurements with the normalized view geometry. The SBAF values are summarized in Table 2. Using the SBAF values, the SR of NewSat was derived as $\rho\rho_{NNccNNRRNNNN} = \rho\rho_{MMMMMMMMRR} * RRSSSSSS$. The TOA reflectance/radiance was then recalculated at the NewSat bands, which served as the reference for absolute radiometric calibration.

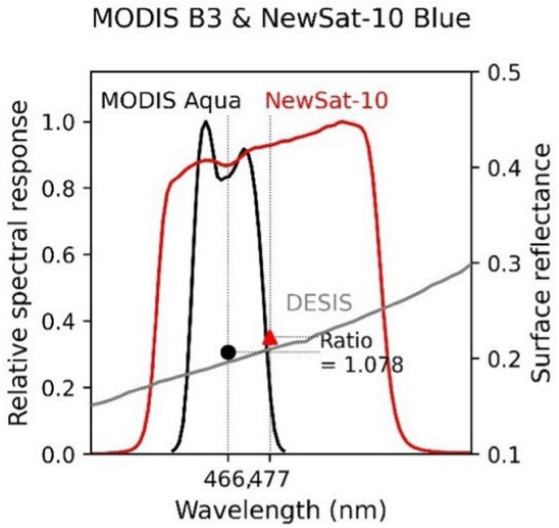

Figure 7. Relative spectral responses of the MODIS Band 3 (B3 centered at 466 nm, black solid line) and the NewSat-10 Blue band (red solid line), along with DESIS hyperspectral surface reflectance (gray solid line). Also shown are the corresponding surface reflectance values for MODIS (black dot) and NewSat-10 (red triangle) estimated from DESIS hyperspectral surface reflectance, as well as the derived SBAF for the Blue band (indicated as 'Ratio').

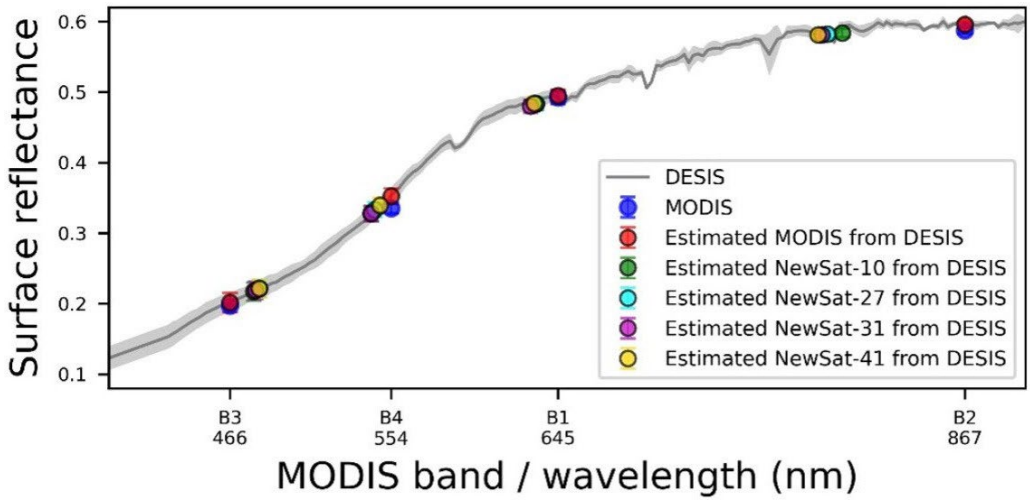

Figure 8. Surface reflectance of DESIS (black line), MODIS (blue circles), and derived for MODIS (red circles) and NewSat (SN)-10 (green), -27 (cyan), -31 (purple), and -41 (yellow) satellites using DESIS hyperspectral measurements over Libya 4.

Table 2. SBAF values for the surface reflectance between MODIS and Satellogic NewSat over Libya 4.

Satellogic Sensor (Generation)	Blue / MODIS B3	Green / MODIS B4	Red / MODIS B1	NIR / MODIS B2
NewSat-10 (Mark IV)	1.078	0.931	0.977	0.980
NewSat-27 (Mark IV)	1.098	0.946	0.977	0.977
NewSat-31 (Mark IV)	1.086	0.930	0.970	0.976
NewSat-41 (Mark V)	1.099	0.964	0.978	0.976

To quantify the relative calibration between NewSat and MODIS, we introduced the sensor gain as the scaling factor between the two measurements. Here, a linear model with a zero-offset involved the assumption: $RR_{NNccNNRRNNNN} = RR_{rrccrr} * gggggggg$, where RR_{rrccrr} is TOA radiance or reflectance from the calibration reference (in this case, MODIS), and $RR_{NNccNNRRNNNN}$ is the corresponding measurement from Satellogic NewSat. If the NewSat sensor is well-calibrated and closely aligned with the MODIS reference, the gain should be close to 1. This is discussed further in the results section that follows. It is important to note that the zero-offset assumption is valid only if the dark frame calibration is accurate, which was not part of this assessment. Dark frame calibration is the process of measuring and removing the sensor electronic noise that appears even in the absence of light. Note that Satellogic performs dark frame calibration on orbit by averaging a series of nighttime ocean captures (Satellogic, 2025a). Satellogic has also stated that vicarious calibration is performed only to adjust gain values while keeping the bias as zero (Satellogic, 2025a).

4.1.2 Results Compliance

Grade: Good

Figure 9 summarizes sensor- and band-specific gain values for the evaluated satellites. The three Mark IV satellites (NewSat-10, -27, and -31) exhibit similar spectral trends: higher gains in the Blue and NIR bands, lower gains in the Green band, and the lowest gains in the Red band. Among them, NewSat-10 shows the highest gain values, particularly in the Blue band, that also has the largest variability (1.182 ± 0.08). The NIR bands for all three satellites exceed a gain of 1.1, indicating that NewSat Mark IV sensors overestimate top-of-atmosphere (TOA) radiance by more than 10% in this portion of the spectrum. All Blue bands also show an overestimation, especially from NewSat-10 and -27, with gain values ≥ 1.1. In contrast, NewSat-27 and -31 demonstrate better absolute radiometric accuracy in the Green and Red bands, with gain values ranging from 0.97 to 1.01. NewSat-31, exhibits the best overall radiometric calibration accuracy among the Mark IV sensors. The Mark V satellite, NewSat-41, shows more consistent absolute radiometric calibration across the Blue, Green, and Red bands, with gain values ranging from 1.03 to 1.05. However, the NIR band presents a significantly higher gain value of 1.15.

These results are useful to understand when considering the accuracy stated by the vendor. According to Satellogic, the overall absolute radiometric accuracy has been evaluated at 10% based on vicarious calibration campaigns conducted at the RadCalNet sites, Railroad Valley Playa (USA), Gobabeb (Namibia), Baotou Sand (China), and La Crau (France) (Satellogic, 2025b). Note that Satellogic updated the radiometric accuracy to 15% following our evaluation. In summary, 11 out of the 16 bands evaluated (4 satellites × 4 bands) fall within ±10% of the ideal gain value of

1.0. Based on the guideline criteria that the mission performance is in good agreement with validation results, the overall grade assigned for absolute radiometric calibration is "Good".

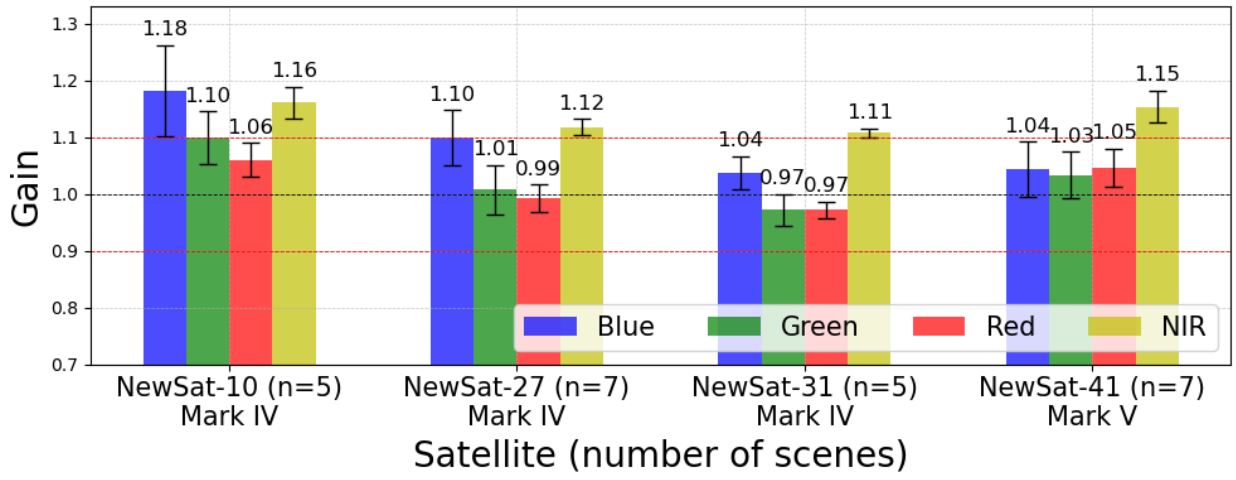

Figure 9. Summary of gain for NewSat-10, 27, 31, and 41 over Libya 4. Satellite names and the number of scenes used are indicated on the x-axis. Mean gain factors are shown as bars with corresponding numeric labels, and the standard deviations are represented by whiskers. A reference gain value of 1 is shown as a black horizontal line, with ±10% bounds indicated by red lines.

4.2 Signal-to-Noise Ratio

4.2.1 Method

The signal-to-noise ratio (SNR) is defined as the ratio of mean signal ($\mu\mu$) to standard deviation of the signal ($\sigma\sigma$), thus $RRSSRR = \mu\mu/\sigma\sigma$. SNR is used to quantify noise in a measurement system. It is typically evaluated during the instrument's pre-launch characterization phase. After launch, this performance can be routinely validated on orbit through various methods that assess the statistical variability of repeated measurements. In the scientific community, two types of SNR are commonly considered: temporal SNR and spatial SNR. However, quantifying temporal SNR from satellite observations is challenging due to the difficulty of acquiring multiple frequent measurements over the same target within a short time window. Therefore, this study focuses on spatial SNR, evaluated over the homogeneous 1×3 km² area located at the Libya 4 pseudo-invariant calibration site.

The methodology for estimating spatial SNR is summarized below:

1) Each band image is divided into 5×5 pixel windows (n = 170,800).
2) For each window, the mean ($\mu\mu$) and standard deviation ($\sigma\sigma$) of TOA reflectance are computed.
3) A histogram of σ is then generated, and the 5th–15th percentile range is used to identify the most homogeneous regions.
4) The scene-level SNR is calculated as the average μ/σ within this range, and the final SNR is obtained by averaging the scene-level values across all available scenes.

We use the 5th–15th percentile range of $\sigma\sigma$ to minimize residual surface variability while excluding potential artifacts. This technique is effective for extracting sensor-related noise more effectively. The entire process is illustrated in Figure 10.

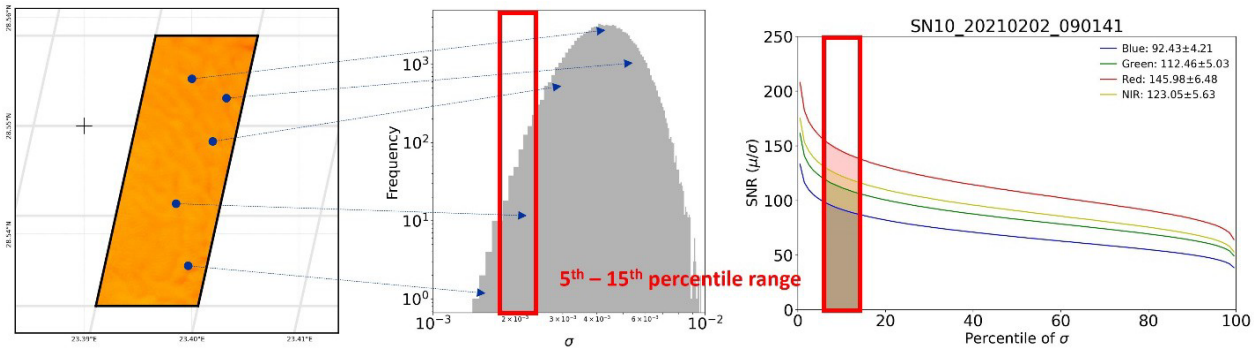

Figure 10. Illustration of the methodology of SNR analysis. In left panel, blue points represent an example set of five 5×5 pixel spatial windows within the 1km x 3km evaluation site. The center panel shows a histogram of the standard deviation ($\sigma\sigma$) collected from the entire set (n=170,800) of 5×5 spatial windows. The right panel shows the SNR ($\mu\mu/\sigma\sigma$) values across the full percentile range of $\sigma\sigma$. In the center and right panels, the red boxes correspond to percentile range (5th-15th percentile of $\sigma\sigma$) for which the final SNR calculation is reported in this evaluation.

The ESA Earthnet Data Assessment Pilot (EDAP) quality assessment report on Mark-IV NewSat data stated a Satellogic SNR claim of 100 at a TOA reflectance of 0.5, regardless of spectral band (Saunier and Kocaman, 2024). Based on this claim, we have defined the grading criteria for NewSat SNR as follows:

- Basic: Fewer than 50% of the spectral bands have SNR higher than 100.
- Good: More than 50% of the spectral bands have SNR higher than 100.
- Excellent: All spectral bands have SNR higher than 100.
- Ideal: All spectral bands have SNR higher than 200.

These criteria are in line with the guideline criteria that the claimed mission performance shows good agreement with validation results. Note that the SNR might depend on the area of interest, since it generally varies with reflectance (e.g., lower SNR from dark ocean). Therefore, this grading criteria is only valid for evaluations over Libya 4 and may not be valid for the full range of land cover types that are of interest to science users.

4.2.2 Results Compliance

Grade: Good

Similar to the absolute radiometric calibration results, the signal-to-noise ratio (SNR) also exhibits consistent spectral trends among the three Mark IV satellites (Figure 11). The Red band shows the highest SNR values, ranging from 123 to 158, followed by the NIR, Green, and Blue bands. All Red bands exceed the SNR threshold of 100, while the Blue bands exhibit the lowest SNR values, ranging from 71 to 91.

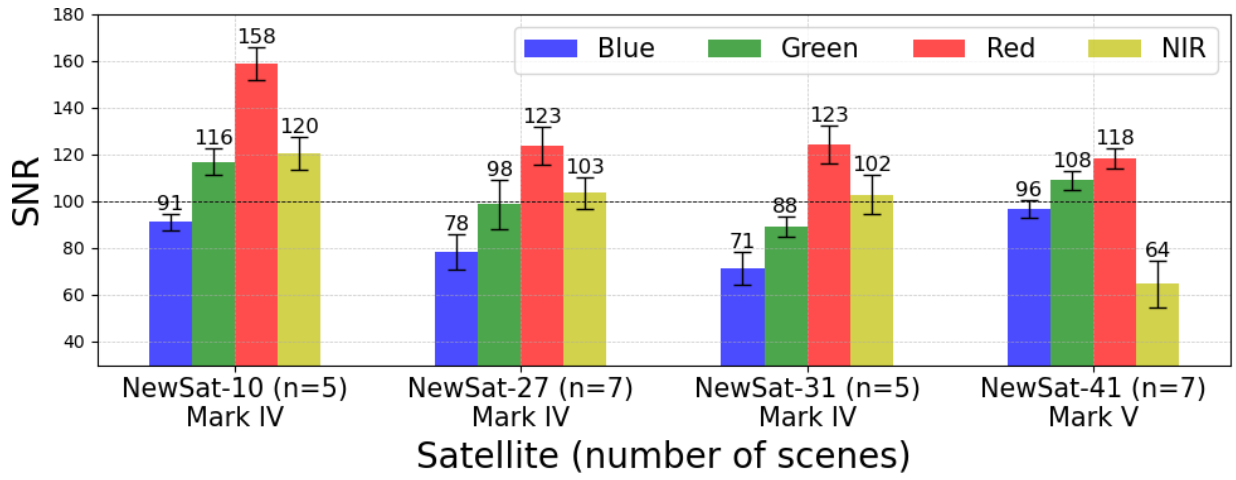

Figure 11. Summary of the SNR for NewSat-10, 27, 31, and 41 over Libya 4. Satellite names and the number of scenes used are indicated on the x-axis. Mean SNR values are shown as bars with corresponding numeric labels, and the standard deviations are represented by whiskers. A reference SNR of 100 is shown as a horizontal line.

The Mark V satellite, NewSat-41, demonstrated more consistent SNR performance across the Blue, Green, and Red bands, with values ranging from 96 to 118. Notably, its Blue band SNR (96) is higher than that of any Mark IV satellite. However, the NIR band of NewSat-41 shows a significantly lower SNR (64), which is the lowest among all 16 analyzed bands. These patterns closely align with the observed trends in absolute radiometric calibration accuracy.

We note that the SNR values from our analysis are slightly higher than those reported in the ESA EDAP report (96–118 vs 79–103), despite the fact that both analyses used the Libya 4 site (Saunier and Kocaman, 2024). This difference can be attributed to two main factors. First, the EDAP report analyzed just one Satellogic satellite (NewSat-30), a Mark IV generation satellite, as the Mark V series had yet to be launched at the time of their study. Secondly, the SNR values in the EDAP report were derived using all Libya 4 pixels in areas with terrain relief, whereas our analysis focused on the most homogeneous pixels, based on spatial standard deviation to avoid shadows due to terrain relief in the Libya 4 sand dunes.

In summary, 9 out of the 16 bands exhibit SNR values greater than 100. Based on this result, and the criteria mentioned in the previous section, the assigned grade for SNR performance is "Good."

Note that we also observed a noticeable discontinuity in the SNR of NewSat images. We calculated $\mu\mu$, $\sigma\sigma$, and $\mu\mu/\sigma\sigma$ and analyzed their spatial distribution over the Libya 4 site (Figure 12). The distribution of $\mu\mu$ does not show any significant discontinuity across the swath. However, the standard deviation ($\sigma\sigma$), computed within each 5×5 pixel box, exhibits abrupt changes along image tile boundaries (appearing as horizontal lines) and frame boundaries (seen as oblique lines). Note that image tiles are combined horizontally, whereas frames are collected consecutively in the along-track direction. These discontinuities propagate into the $\mu\mu/\sigma\sigma$ distribution and ultimately affect the SNR. This issue was observed across all bands and all satellites. According to the ESA EDAP report, which originally reported SNR discontinuities, the discontinuities may be caused by equalization processing between image frames and images combined into tiles (Saunier and Kocaman, 2024). This behavior appears to be related to the image compositing process described

by the vendor, which can cause sharp intensity transitions between adjacent frames. We suspect that the observed discontinuities in μ/σ and SNR distributions are linked to this compositing issue.

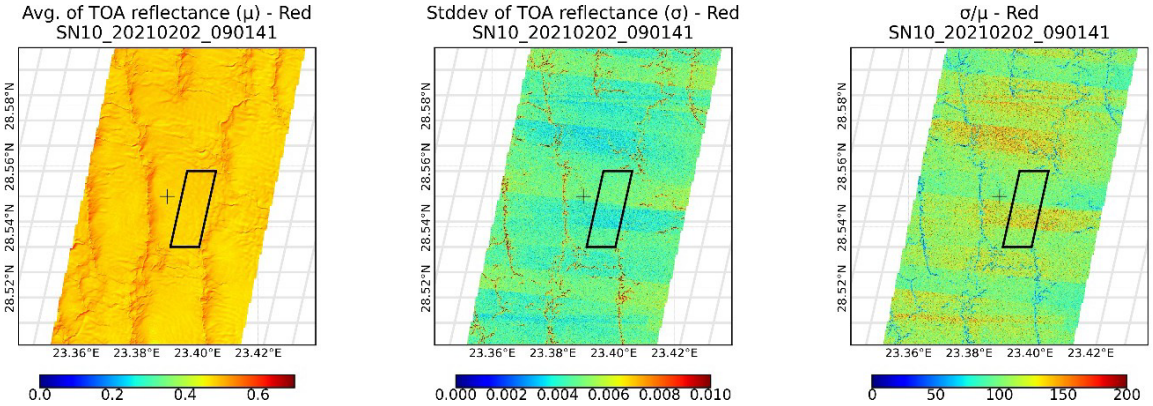

Figure 12. Distribution of mean ($\mu\mu$; left), standard deviation ($\sigma\sigma$; center) and $\sigma\sigma/\mu\mu$ (right) of the 5×5 pixel boxes ("small windows") over Libya 4. The images are from NewSat-10 Red band measurements on Feb-02, 2021 at 09:01:41 UTC. The black extent shows the 1km x 3km evaluation site.

4.3 Temporal Stability

4.3.1 Method

Even if a sensor is well-calibrated in the laboratory prior to launch, its radiometric characteristics can drift over time in orbit. Therefore, continuous validation is essential to monitor and maintain its radiometric calibration throughout the mission. Most commercial satellites, including the Satellogic NewSat series, are not equipped with onboard calibration systems such as a solar diffuser or a solar diffuser stability monitor. Instead, they generally rely on inter-sensor comparisons with reference satellite instruments and various vicarious calibration methods. According to Satellogic, NewSat calibration relies on cross-comparison with Sentinel-2 data, including spectral band adjustments. However, the publicly available documentation does not specify how frequently this cross-calibration is performed or whether it is used to regularly update sensor gains (Satellogic, 2025a).

To assess the temporal stability of radiometric calibration, TOA radiance or reflectance measurements obtained under varying viewing geometries must be converted to a common viewing geometry. As described in the methodology for absolute calibration assessment, the MDCA processing includes BRDF normalization to convert TOA reflectance/radiance to a standardized geometry, specifically, a solar zenith angle of 20° and a nadir sensor view. This involves the following steps:

1. Atmospheric correction using MODIS MAIAC atmospheric parameters,
2. Conversion of surface reflectance to a normalized viewing geometry using MODIS MAIAC BRDF shape, and
3. Calculation of TOA reflectance/radiance at the normalized geometry.

Using this approach, NewSat TOA reflectance measurements were converted to the normalized viewing geometry. Similarly, reference MODIS TOA reflectance values were computed at the same geometry and spectrally adjusted to match the NewSat band characteristics. Given that the Libya 4 site is quasi-stable and typically exhibits low aerosol loading, we assume that TOA reflectance at the normalized view geometry remains temporally invariant over the analysis period. Note that the original NewSat pixels were aggregated to 1×1 km² MODIS grids for analysis, as described in the absolute radiometric calibration section.

There is no specification in the Satellogic NewSat documentation about temporal stability. We thus devised the following grading criteria for temporal stability for NewSat as follows:

- When the number of samples is insufficient (fewer than 10) or the temporal coverage is less than one year:
    - Basic: Noticeable trends are observed through visual inspection.
    - Good: No noticeable trends are observed through visual inspection.
- When the number of samples is sufficient (10 or more) and the temporal coverage exceeds one year:
    - Basic: Temporal trend exceeds ±5% per year
    - Good: Temporal trend is within ±5% per year
    - Excellent: Temporal trend within ±1% per year
    - Ideal: Temporal trend within ±0.5% per year

4.3.2 Results Compliance

Grade: Good
Figure 13 presents a time series of TOA reflectance at a normalized viewing geometry for each set of NewSat sensor images acquired for assessment. NewSat measurements (dots with solid lines) exhibit greater variability compared to the reference MODIS data (triangles with dashed lines), particularly during short periods in early February 2021 for NewSat-10 and May 2024 for NewSat-41. However, none of the NewSat satellites show any noticeable trends upon visual inspection, and the observed variation appears to fall within the expected measurement uncertainty, the assigned grade for temporal stability is “Good.”

We did not attempt to extract linear temporal trends in TOA reflectance, as the number of observations per sensor (typically 5–7) is insufficient to robustly assess temporal variability. Additionally, the observation periods over Libya 4 were relatively short, approximately 1.5 months for NewSat-10 and 6 months for NewSat-41, further limiting a trend analysis.

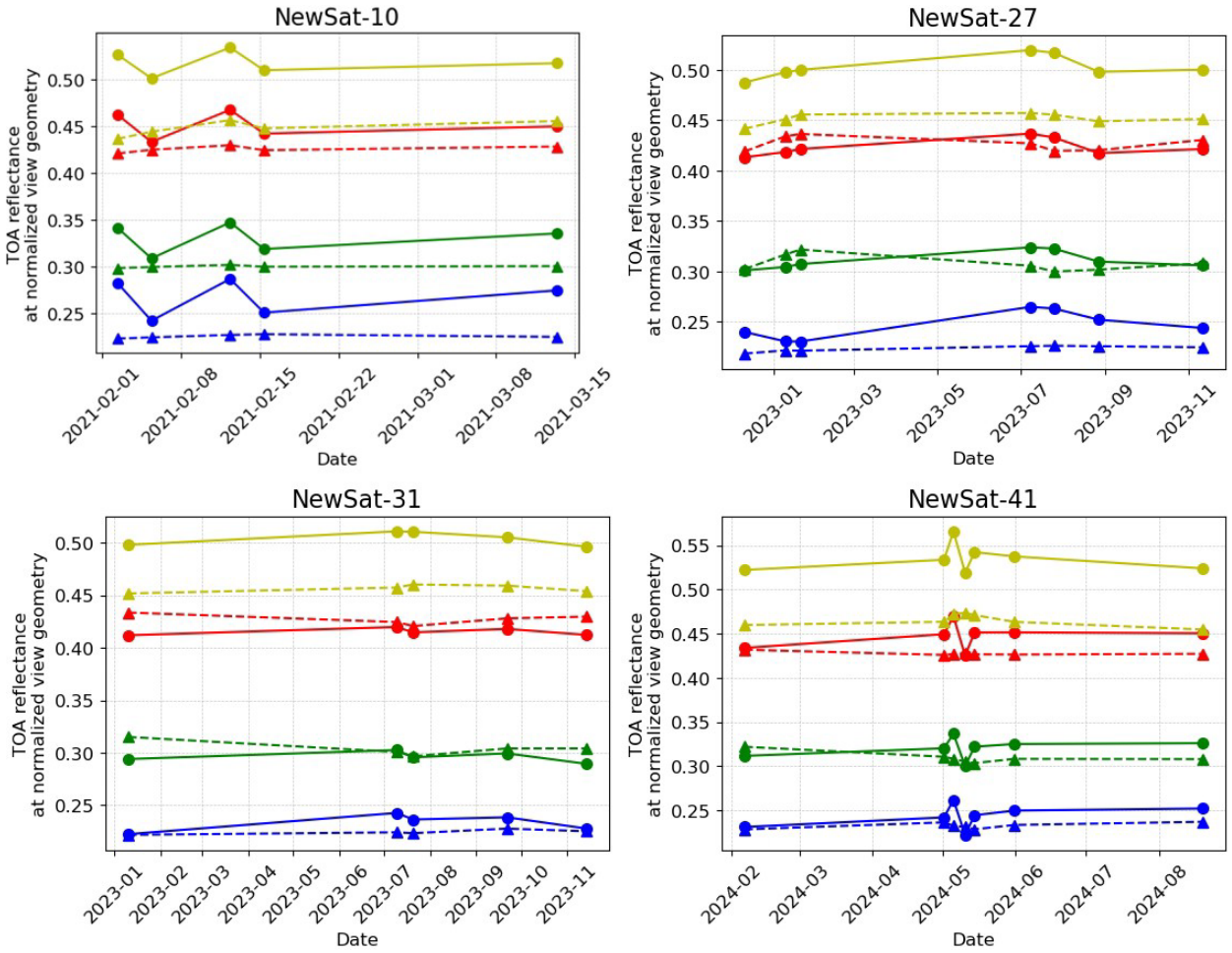

Figure 13. Time series of top-of-atmosphere reflectance at normalized viewing geometry (nadir view; solar zenith angle of 20°) over Libya 4 site. Circles with solid lines represent NewSat measurements, while triangles with dashed lines denote the MODIS reference data. The Blue, Green, Red, and NIR bands are shown in blue, green, red, and yellow, respectively. Three are Mark IV, only NewSat-41 is Mark V generation data. The TOA reflectance of the NewSat data is aggregated (mean) here to the much larger spatial resolution of the corresponding MODIS pixel extent.

5 Detailed Validation – Geometric

5.1 Sensor Spatial Response

5.1.1 Method

The assessment of sensor spatial response (SSR) uses three related functions to describe the spatial fidelity of satellite imagery. The Edge Spread Function (ESF), the Line Spread Function (LSF), and the Modulation Transfer Function (MTF) are all related measurements. The ESF measures how sharply a sensor captures transitions between bright and dark areas, the LSF is the derivative of ESF showing the sensor's response to a thin line, and MTF is the Fourier transform of LSF that quantifies how well the sensor preserves contrast at different spatial frequencies. The MTF at the Nyquist frequency (half the sampling rate) is particularly critical for satellite imagery because it indicates whether the sensor can resolve the finest details possible given its pixel size - values

above 0.3-0.4 generally indicate adequate spatial resolution for distinguishing adjacent features without significant image degradation. We applied these functions to images over the Baotou, China calibration and validation site (109.628°E, 40.854°N) where large high-contrast (checkerboard) features are maintained for analysis of in-flight sensor radiometric and spatial performance. The checkerboard is a set of black and white squares (48×48 m) that are slightly slanted with respect to the image grid direction. Six NewSat images over Baotou were ordered for this analysis, two from the older Mark IV generation, and four from the Mark V generation. The sensors evaluated were the Mark IV NewSat-27 and -31, as well as the Mark V NewSat-41, -43, -48, and –50 (Table A2). The Satellogic images assessed were the TOA L1D-ortho product.

For each image direction along-row or along-column, the assessment starts with reading in 20 x 20 rows and columns across the black/white (B/W) transition (Fig 14a). A transition line location is initially estimated based on visual inspection of each image and is refined later with the extracted data. Pixels are then transformed from bins to distance (Fig. 14b) from the transition line, with the equation $d_p = d*\cos(\Theta)$, where Θ is the angle between the line and vertical/horizontal, d is the vertical/horizontal distance from the pixel center to the transition line, and d_p is the perpendicular distance from the pixel center to the transition line.

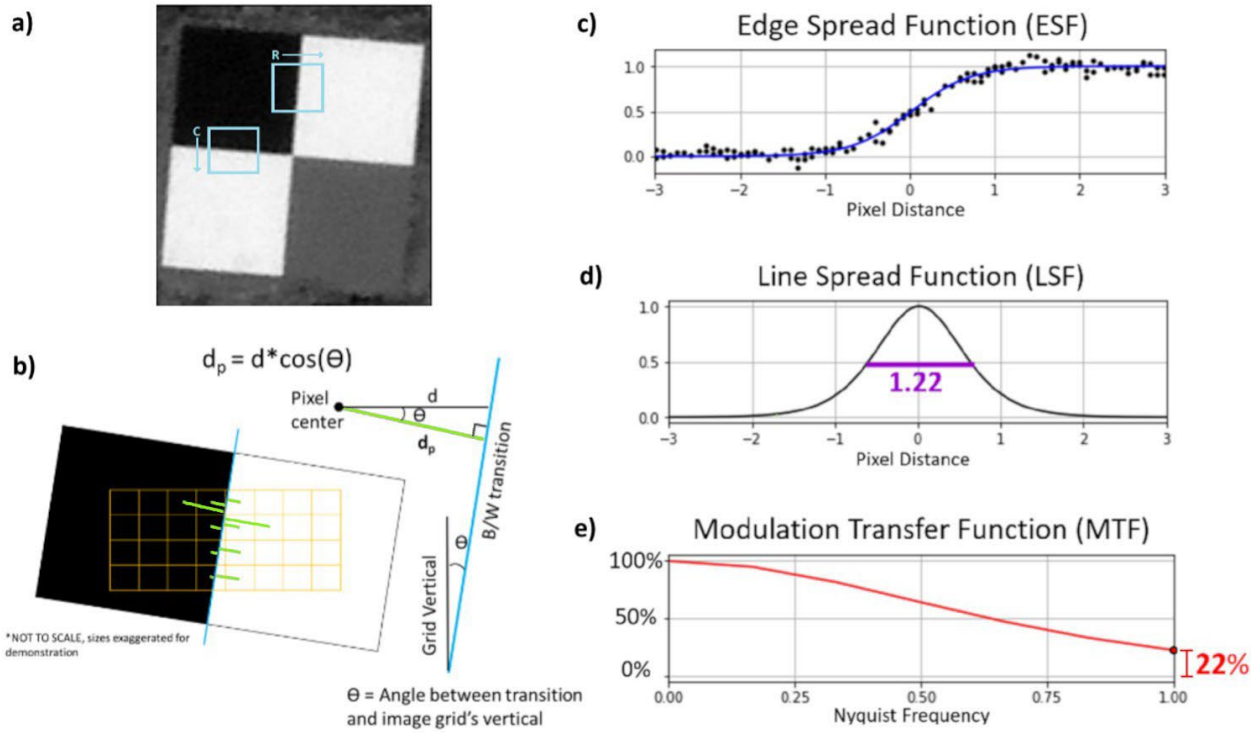

Figure 14. Visual demonstration of our SSR calculations. a) A NewSat image (Red band - 20241026_034500_SN50) over Baotou, China site. Blue overlay squares indicate regions used in edge spread calculations in the row (R) and column (C) directions. b) The sub-pixel resolution is calculated based on the distance to the pixel centers (green lines) from the black/white transition. The sample graphic here is showing the row direction. c) The pixel edge response is constructed based on the distance calculations shown in (b) and a polynomial fit (blue) for the ESF. d) The LSF is the derivative of the ESF (c). The full width at half maximum (FWHM) = 1.22 pixels, the pixel footprint size, and is marked with a purple line. e) The MTF is the Fourier transform of the LSF (d). Here, the x-axis is normalized by Nyquist frequency of 1 cycle in 2 pixels. The MTF of this image is 22%.

Once the values are transformed into distance from the B/W transition, a polynomial is fit to the line, creating an ESF (Fig. 14c). The derivative of the ESF is the LSF (Fig. 14d) in the direction of interest. The Full Width at Half Maximum (FWHM) is found from this LSF to represent the sensor's effective footprint size. Finally, the normalized magnitude of the Fourier transform of the LSF gives the MTF (Fig. 14e). One more metric for spatial response is found with the MTF curve, the MTF value at Nyquist frequency (Fig. 14e, red dot). MTF is a numerical representation of how much contrast on the ground is captured by the sensor. In the case of Figure 14, this image retains 22% of the original ground contrast. This is a good retention because features that vary at the pixel level will be distinguishable at 10% - 25% contrast retention. At lower than 10%, features that vary at the pixel level will not be reproduced in the image. We will evaluate the Satellogic NewSat spatial response with FWHM as its effective footprint size.

Six out the 16 Satellogic sensors acquired for geometric assessment were evaluated for the SSR evaluation. Of these, two were from Mark IV sensors, and four were from Mark V generation sensors.

5.1.2 Results Compliance

Grade: Excellent (Mark IV), Basic (Mark V)
The NewSat Mark IV average spatial resolution expressed in FWHM of the LSF is 1.45 pixels in the row direction and 1.56 pixels in the column direction. The quality criteria in the assessment guidelines for SSR are based on the ratio of the FWHM to the ground sampling distances (GSD), or pixel resolution. Table 3 shows a summary of our SSR assessment findings. The Blue and Green bands perform the best at ~ 1 pixel, while the NIR band has a consistently coarser spatial resolution at ~ 2 pixels. The Red band is consistently coarser than the Blue and Green bands but is sharper than the NIR band.

Table 3. Calculated NewSat mean sensor spatial resolution by band, in pixels. Row and column direction SSR are averaged here. The NIR band considerably underperforms compared to the other bands, even more so for Mark IV.

Satellite Generation	FWHM (pixels) Mean (Standard Deviation)					Assessment Grade
	NIR	Red	Green	Blue	Overall	
Mark IV	2.15 (0.07)	1.41 (0.14)	1.11 (0.03)	1.05 (0.07)	1.43 (0.46)	Excellent
Mark V	3.34 (0.42)	3.06 (0.43)	2.85 (0.47)	2.76 (0.44)	3.00 (0.47)	Basic

The NewSat Mark V average spatial resolution, expressed in FWHM of the LSF, is 2.94 pixels in the row direction and 3.06 pixels in the column direction. The Blue and Green bands perform the best at ~2 pixels, while the NIR band has a consistently coarser spatial resolution at ~3 pixels. The Red band is consistently coarser than the Blue and Green bands but sharper than the NIR band.

The SSR of the NewSat sensors differs by generation. The Mark IV SSR grade is "Excellent" because the ratio of the average sensor spatial response to pixel size is 1.43, between 1.25 and 1.5, which is criteria for "Excellent." The Mark V SSR grade, however, is "Basic" because the ratio of the average sensor spatial response to pixel size is 3.0, and the criteria state that any ratio above 2

is considered “Basic.” Both generations have a slightly larger spatial response in the column direction than the row direction.

Each sensor performs slightly differently, Appendix Table A3 contains the details of all the sensor spatial responses evaluated.

5.2 Absolute Positional Accuracy

5.2.1 Method

The evaluation of the Satellogic NewSat absolute positional accuracy (APA) is in fact a relative assessment. The georeferenced panchromatic band of the Maxar WorldView (WV) -2 and -3 sensors were used as the reference for the NewSat geolocation accuracy assessment. The WV panchromatic band used as reference imagery have resolutions ranging from 0.3 m - 0.8 m, according to their metadata. The WorldView imagery has a CE90 of 5.4 m [DigitalGlobe Inc, 2016]. The WorldView data were orthorectified using the Shuttle Radar Topography Mission (SRTM) digital elevation model (DEM) dataset (30 m). The CSDA program purchased the Satellogic orthorectified image products (L1D) for the evaluation.

The locations used to evaluate positional accuracy included urban infrastructure that exhibit little relief displacement (structures within cities and airports). These locations follow our criteria of an areal overlap with the reference data of at least 3 km^2 in size with minimal tree cover, low buildings, and no cloud cover. At very high resolution, changes in tree canopy cover and building shadows interfere with the image matching algorithm. Note that our evaluation site criteria are considered a best-case scenario at locations with easy-to-match features. It should also be noted that many science teams work in remote locations where feature matching is challenging, and thus they can expect lower geolocation accuracy than what is reported here.

For each location, the assessment starts by determining the overlap between the reference and target images. This overlap region is then split into subset images of 250×250 m chips. Each chip in the target image has a matching chip in the refence image based on the image geolocation metadata. The algorithm then imposes offsets on the target chip of the pair and calculates the Pearson Cross Correlation (PCC) coefficient (a measurement of how well two images match). The offsets that give the best PCC are taken to be the geolocation offsets between the chip pair. The quality of chip co-registration is then calculated with a measurement uncertainty equation [De Luccia et al. 2016] that is used to filter out poor quality chip matches [Semple et al, 2023]. Each site featured a range of 68 – 2680 chips used to assess the absolute positional accuracy. At least 20 high quality (low standard deviation) chips are required for an accurate analysis, which all the locations met.

The orthorectified Maxar WV imagery served as the geolocation reference, which have their own geolocation uncertainty. A minimum of 5 WV reference images were selected per location. To overcome the positional uncertainty in the reference data, we selected a central reference image at each site to use as the final reference for assessing NewSat image positional accuracy. This removed a potential bias due to instability in the WV geolocation accuracy.

The metrics we calculate include the standard CE90 and a modification, referred to as the CE90-demean. The CE90 is the 90th percentile of the circular error of target image chip offsets relative to the reference, which is considered the 'truth'. That is, 90% of the measured errors are within that value, while 10% of the errors exceed that value. The CE90-demean is similar to the standard CE90 calculation but assumes there is no systematic bias between the NewSat and WV reference images. CE90-demean measures the uncertainty of the Satellogic geometric calibration system, in other words their self-consistency. It also accounts for possible biases in using different reference points from those that Satellogic uses. Figure 15 shows a visual demonstration of CE90 vs CE90-demean where the two metrics are different.

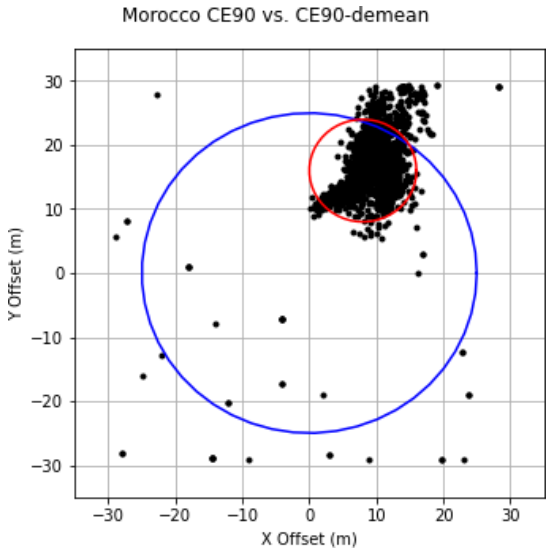

Figure 15. The CE90 (blue circle) and CE90-demean (red circle) difference for the Morocco site shows grouping of evaluated Satellogic offsets (black points) off-center from the reference WV image.

5.2.2 Results Compliance

Grade: Basic
Satellogic claims a CE90 of 10 m for NewSat sensors. The evaluation criteria state that the grading of APA for very high-resolution data is "Basic" if the CE90 is outside the vendor's specification.

We found that the sensor geolocation accuracy of the NewSat Mark IV and Mark V generations do not meet their CE90 claim, when considered globally, relative to WorldView, however it does meet this claim relative to NewSat data. Both Table 4 and Figure 16 show the global offsets when considering CE90 (a, b) and CE90-demean (c, d). Overall, the NewSat Mark IV images have an average CE90 of 17.4 m, and average CE90-demean of 9.7 m. The NewSat Mark V images have an average CE90 of 17.0 m, and an average CE90-demean of 9.3 m. The NewSat CE90 is within specification for just 1 of 5 locations evaluated for Mark V, while the average CE90-demean is within specification for 4 out of the 5 locations. For Mark V, the CE90 was not within specification for any of the Mark V locations evaluated, while the average CE90-demean was within specification for 3 of the 4 locations.

The full results for the positional accuracy for the Satellogic NewSat imagery we assessed are given in Appendix Tables A4 and A5.

Table 4. Summary of APA (CE90) and self-consistency (CE90-demean) for each generation.

NewSat Generation	APA (m)	APA (Pixels)	APA Grade	Self-consistency (m)	Self-consistency (pixels)	Self-Consistency Grade
Mark IV	17.4 m	~18 pixels	Basic	9.7 m	~10 pixels	Good
Mark V	17.0 m	~24 pixels	Basic	9.3 m	~13 pixels	Good

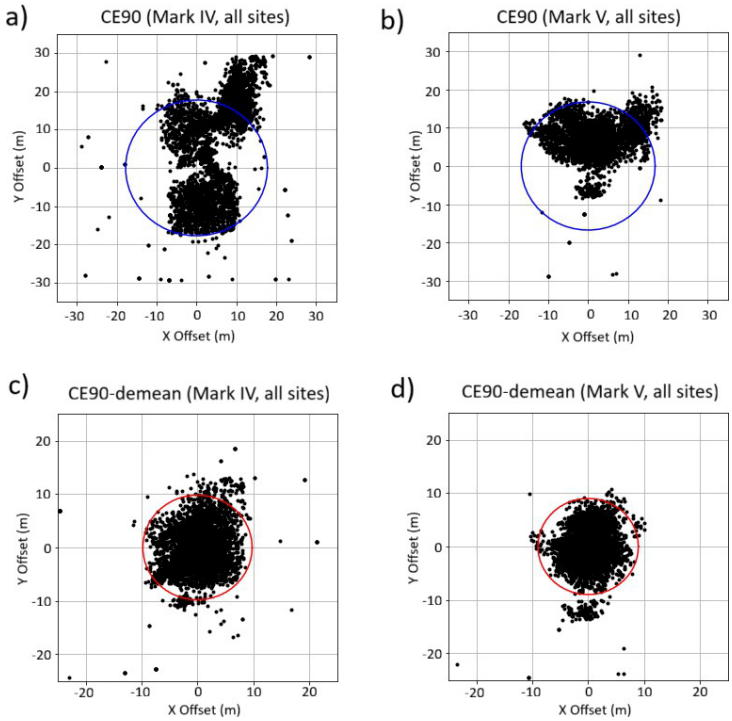

Figure 16. A summary of the relative offsets for Mark IV (a, c) and Mark V (b, d) satellites across all 5 sites show CE90 (top row, blue circle) and CE90-demean (bottom row, red circle). Valid matches are plotted as black dots.

5.3 Band-to-Band Registration

5.3.1 Method

Band-to-band registration (BBR) was assessed with the image matching algorithm that is described in Section 5.2.2. Each band of an image is assessed using its corresponding Red band image as the reference.

5.3.2 Results Compliance

Grade: Excellent (Mark IV), Ideal (Mark V)
The Satellogic NewSat sensors use a butcher-block-like patterned RGBN (Red, Green, Blue, and NIR) color filter array. As such, band acquisition timing is not simultaneous. When the individual RGBN images are combined, a time difference is introduced into the final multi-band dataset. This acquisition design results in expected band offsets of fast-moving objects such as vehicles and clouds.

The Satellogic documentation specifies a different BBR for the Mark IV and Mark V generations. Their specification for Mark IV BBR is <2 m and for Mark V is <1.4 m. Our evaluation of both generations indicate that they meet and exceed this specification (Table 5). According to the assessment guideline criteria, the NewSat Mark IV BBR grade is "Excellent" because the band pair overlap area is less than or equal to 90% but greater than 64% footprint area. Their Mark V generation grade is "Ideal" because the band pair overlap area is greater than 90% footprint area. The BBR quality improved with the newer generation Mark V sensors.

Table 5. BBR offsets found for both Satellogic NewSat sensor generations.

Sensor Generation	BBR (m)	Overlap Area	Grade
Mark IV	0.40 m	82%	Excellent
Mark V	0.32 m	90%	Ideal

5.4 Temporal Stability

5.4.1 Method

The temporal stability of the positional accuracy and precision was assessed using the image matching algorithm that is described above in section 5.2.2. We acquired 10 NewSat images spanning a 4-year period from 2021–2025 over the Morocco site for the temporal stability assessment. The most recently acquired NewSat image in the set was used as the reference image. At locations where a long time series was not available, we use the CE90-demean as a temporal stability metric, as explained below.

5.4.2 Results Compliance

Grade: Good
Satellogic does have a temporal stability claim for NewSat beyond their geolocation accuracy specification of 10 m CE90. Based on CE90-demean, a metric for NewSat self-consistency, the Mark IV data from the Argentina and Morocco sites performed similarly, at 8.6 m and 9.0 m respectively, and are within specification. We only obtained one image each for the New Mexico and Sicily site locations from Mark IV, thus a CE90-demean assessment could not be performed. For the Mark V data, the Morocco, New Mexico and Sicily CE90-demean were 6.7 m, 6.6 m, and 7.4 m, respectively, and were all self-consistent. The Singapore location did not have enough Mark V acquisitions for the CE90-demean assessment. The summary of Mark IV and Mark V CE90 and CE90-demean are shown in Table 6, with further details of the assessment provided in Appendix tables A4 and A5.

Table 6. Temporal Stability Summaries by Site for NewSat Mark IV and Mark V generations. Highlights indicate locations with CE90 larger than the specification of CE90 < 10 m.

Sites	Mark IV		Mark V	
	CE90	CE90 Demean	CE90	CE90 Demean
Argentina	9.4	9	N/A	N/A
Morocco	25.3	8.6	20.6	6.7
New Mexico	16.1	N/A	10.8	6.6
Sicily	17.4	N/A	16.1	7.4
Singapore	18.9	15.3	20.4	N/A
Mean	**17.4**	**9.7**	**17.0**	**9.3**

Temporal stability at the Morocco site for both the Mark IV and Mark V generations is plotted in Figure 17. Both the north-south offsets (black triangles) and east-west offsets (blue circles) were used to indicate the direction of the temporal shifts. Here, 8 of the 10 images acquired were from the Mark IV generation. When considered across generations, the offsets here exceed the specification of 10 m CE90.

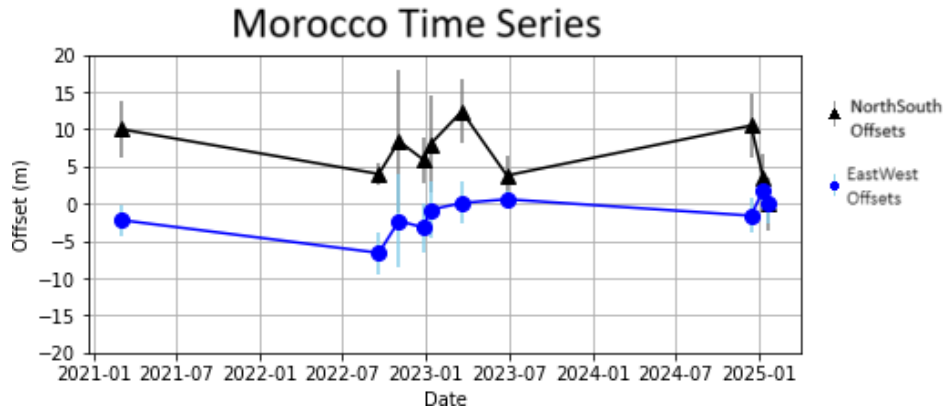

Figure 17. Time series stability analysis at the Morocco site. Offsets are relative to the final image in the time series. The last two images are from the Mark V generation, the other eight are from the Mark IV generation. The north-south offsets are plotted as black triangles with grey standard deviation bars and range from 0 m to 12 m from the final image. The east-west offsets are plotted as blue circles with light blue standard deviation bars and range from 2 m to -7 m from the final image.

The Satellogic NewSat time-series analysis is within specification, thus the Satellogic temporal stability grade is "Good." However, we note that none of the locations reviewed performed well enough for a time series analysis. The geolocation accuracy varies on a scale of tens of pixels over the 4-year timeline of this dataset, which is too large for most scientific applications. Before performing a time-series analysis, users will either need to rectify the images to within a single pixel accuracy, using a reference image, or aggregate the pixels by an appropriate aggregation scheme (such as 10×10).

6 Summary

The CSDA Program SMEs conducted an evaluation of the Satellogic NewSat constellation from both the Mark IV and V generation of sensors, assessing 60 TOA reflectance images across 7 sites from 17 NewSat sensors spanning 2021-2025. The assessment included both radiometric and geometric performance evaluations, along with a review of the Satellogic NewSat documentation provided. The radiometric assessment analyzed imagery from the Libya 4 pseudo-invariant calibration site, examining radiometric calibration, signal-to-noise ratio (SNR), and temporal stability across four satellites with four spectral bands each. The radiometric results showed that 11 out of 16 bands were within a 10% gain range compared to Aqua MODIS (exceeding "Good" rating criteria). It was also noted that the NIR bands consistently showed the highest gains across all satellites examined in the sample. The radiometric assessment found that 9 out of 16 bands featured SNRs above 100, representing over 50% and meeting a "Good" rating for SNR based on established criteria. However, the temporal stability of the radiometry yielded no statistically significant trends due to low sample numbers. The geometric assessment evaluated sensor spatial response, absolute positional accuracy, band-to-band registration, and temporal stability using sites associated with built up environments, with data from both sensor generations. Geometric performance varied between sensor generations, with Mark IV receiving an "Excellent" grade for sensor spatial response while Mark V received a "Basic" grade, while both generations exceeded their specified sensor spatial response specifications.

7 References

Alonso, K., Bachmann, M., Burch, K., Carmona, E., Cerra, D., de los Reyes, R., Dietrich, D., Heiden, U., Hölderlin, A., Ickes, J., Knodt, U., Krutz, D., Lester, H., Müller, R., Pagnutti, M., Reinartz, P., Richter, R., Ryan, R., Sebastian, I., & Tegler, M. (2019). Data Products, Quality and Validation of the DLR Earth Sensing Imaging Spectrometer (DESIS). *Sensors*, *19*(20), 4471. https://doi.org/10.3390/s19204471

Choi, M., Lyapustin, A., Wang, Y., Tucker, C. J., Khan, M. N., Policelli, F., Neigh, C. S. R., & Hall, A. A. (2024). Calibration of Maxar Constellation Over Libya-4 Site Using MAIAC Technique. *IEEE Journal of Selected Topics in Applied Earth Observations and Remote Sensing*, *17*, 5460–5469. https://doi.org/10.1109/JSTARS.2024.3367250

De Luccia, F. J., Houchin, S., Porter, B. C., Graybill, J., Haas, E., Johnson, P. D., Isaacson, P. J., and Reth, A. D. (2016), "Image navigation and registration performance assessment tool set for the GOES-R Advanced Baseline Imager and Geostationary Lightning Mapper", Proc. SPIE 9881, Earth Observing Missions and Sensors: Development, Implementation, and Characterization IV, 988119 (2 May 2016); doi: 10.1117/12.2229059.

DigitalGlobe Inc. (2016), "Accuracy of worldview products" [White Paper]. Last accessed 15 June 2023. https://dg-cms-uploads-production.s3.amazonaws.com/uploads/document/file/38/DG_ACCURACY_WP_V3.pdf

ESA, NASA (2024), "Earth Observation Mission Quality Assessment Framework - Optical Guidelines". Issue 0.2 (draft), 2024.

Krutz, D., Müller, R., Knodt, U., Günther, B., Walter, I., Sebastian, I., Säuberlich, T., Reulke, R., Carmona, E., Eckardt, A., Venus, H., Fischer, C., Zender, B., Arloth, S., Lieder, M., Neidhardt, M., Grote, U., Schrandt, F., Gelmi, S., & Wojtkowiak, A. (2019). The Instrument Design of the DLR Earth Sensing Imaging Spectrometer (DESIS). *Sensors*, *19*(7), 1622. https://doi.org/10.3390/s19071622

Lyapustin, A. I. (2005). Radiative transfer code SHARM for atmospheric and terrestrial applications. *Applied Optics*, *44*(36), 7764. https://doi.org/10.1364/AO.44.007764

Lyapustin, A., Wang, Y., Xiong, X., Meister, G., Platnick, S., Levy, R., Franz, B., Korkin, S., Hilker, T., Tucker, J., Hall, F., Sellers, P., Wu, A., & Angal, A. (2014). Scientific impact of MODIS C5 calibration degradation and C6+ improvements. *Atmospheric Measurement Techniques*, *7*(12), 4353–4365. https://doi.org/10.5194/amt-7-4353-2014

Lyapustin, A., Wang, Y., Choi, M., Xiong, X., Angal, A., Wu, A., Doelling, D. R., Bhatt, R., Go, S., Korkin, S., Franz, B., Meister, G., Sayer, A. M., Roman, M., Holz, R. E., Meyer, K., Gleason, J., & Levy, R. (2023). Calibration of the SNPP and NOAA 20 VIIRS sensors for continuity of the MODIS climate data records. *Remote Sensing of Environment*, *295*, 113717. https://doi.org/10.1016/j.rse.2023.113717

Satellogic. (2025a). Vicarious calibration. In *Imagery products: Image processing*. Satellogic Developers. Retrieved August 7, 2025, from https://developers.satellogic.com/imagery-products/image_processing.html#vicarious-calibration

Satellogic. (2025b). Radiometric calibration. In *MSI payload specifications*. Satellogic Developers. Retrieved April 29, 2025, from https://developers.satellogic.com/imagery-products/msi_payload_specifications.html#radiometric-calibration

Saunier, S. and Kocaman, S. (2024). EDAP+ TN on Quality Assessment of NewSat/MSI, Issue 1.0, ESA the Earthnet Data Assessment Project (EDAP+), https://earth.esa.int/documents/d/earth-online/technical-note-on-quality-assessment-for-newsat

Semple, A., B. Tan, and G. Lin. (2023), “Automation of Geometric Accuracy Assessment Algorithm”, JACIE 2023 Workshop, USGS, Reston, VA. https://view.officeapps.live.com/op/view.aspx?src=https%3A%2F%2Fcalval.cr.usgs.gov%2Fapps%2Fsites%2Fdefault%2Ffiles%2Fjacie%2F2023-S4-Alana_Semple_Automation.pptx&wdOrigin=BROWSELINK

USGS Spatial Sites Catalog, USGS EROS CalVal Center of Excellence. Last accessed 17 July 2025. https://calval.cr.usgs.gov/apps/spatialsites_catalog

Appendix

Table A1. List of 24 images and associated metadata over Libya 4 used for radiometric calibration evaluation. Co-located reference data used for the evaluation includes MODIS MAIAC aerosol optical depth (AOD), column water vapor, and MERRA-2 total column ozone.

Sensor	Measurement date and time in UTC (YYYYMMDD_hhmmss)	Solar zenith angle (°)	View zenith angle (°)	Sun azimuth angle (°)	View azimuth angle (°)	MODIS MAIAC AOD at 443 nm	MODIS MAIAC CWV (cm)	MERRA-2 TCO (dobson unit)
NewSat-10 Mark IV	20210202_090141	51.11	24.64	149.21	97.70	0.122	1.792	321.689
	20210205_091047	49.36	2.30	151.13	273.39	0.107	1.306	281.368
	20210212_090048	48.53	26.54	146.82	97.50	0.118	0.853	281.857
	20210215_090944	46.58	0.18	148.79	156.81	0.233	1.629	273.963
	20210313_090422	38.26	14.96	141.19	98.28	0.233	1.414	287.457
NewSat-27 Mark IV	20221210_093852	52.37	4.37	168.29	266.64	0.170	1.712	265.462
	20230109_093741	52.40	1.66	163.67	265.11	0.185	1.290	279.989
	20230120_093721	50.79	1.11	161.75	308.11	0.128	1.134	263.106
	20230708_093703	13.68	4.41	113.30	98.69	0.205	2.248	290.027
	20230725_093815	15.29	2.00	122.53	109.16	0.243	2.032	282.705
	20230827_094045	21.54	2.20	146.67	275.13	0.198	2.640	289.217
	20231111_094439	46.36	2.86	171.52	276.13	0.181	1.873	282.467
NewSat-31 Mark IV	20230110_115444	54.14	1.67	203.32	271.70	0.184	1.692	270.125
	20230709_120003	20.87	1.72	257.75	100.92	0.165	2.573	289.464
	20230720_120005	21.31	3.47	253.12	100.60	0.167	1.869	289.090
	20230921_120358	37.39	3.11	226.43	99.28	0.241	2.121	287.480
	20231113_120748	54.45	3.34	214.90	100.71	0.225	1.861	286.292
NewSat-41 Mark V	20240206_115907	48.15	12.95	205.77	99.39	0.070	1.467	314.547
	20240501_120338	26.65	7.14	245.53	100.25	0.500	1.986	295.988
	20240505_121225	27.91	18.56	250.24	278.51	0.274	1.468	334.680
	20240510_115932	24.61	20.06	249.41	98.38	0.287	1.326	320.146
	20240514_120701	25.72	1.78	253.51	273.63	0.154	1.405	304.736
	20240531_120850	24.47	4.40	260.48	274.90	0.194	1.974	332.202
	20240819_121512	29.28	9.73	242.21	277.70	0.211	2.987	283.895

Table A2. List of 36 images from the 5 cities used for the geometric calibration evaluation (locations generalized).

Sensor	NewSat Generation	Measurement date and time in UTC (YYYYMMDD_ hhmmss)	General Location
NewSat-29	Mark IV	20230705_170951	Argentina
NewSat-29	Mark IV	20230801_171901	Argentina
NewSat-27	Mark IV	20230802_145352	Argentina
NewSat-28	Mark IV	20230804_171446	Argentina
NewSat-32	Mark IV	20230828_132552	Argentina
NewSat-31	Mark IV	20230303_062132	China
NewSat-27	Mark IV	20231029_040828	China
NewSat-43	Mark V	20231204_062911	China
NewSat-41	Mark V	20241003_063721	China
NewSat-50	Mark V	20241026_034500	China
NewSat-48	Mark V	20241110_034414	China
NewSat-16	Mark IV	20210303_111934	Morocco
NewSat-24	Mark IV	20220919_115405	Morocco
NewSat-21	Mark IV	20221102_151703	Morocco
NewSat-21	Mark IV	20221226_152524	Morocco
NewSat-21	Mark IV	20230110_152116	Morocco
NewSat-22	Mark IV	20230320_152558	Morocco
NewSat-24	Mark IV	20230627_113430	Morocco
NewSat-34	Mark IV	20241214_102810	Morocco
NewSat-41	Mark V	20250109_142338	Morocco
NewSat-50	Mark V	20250121_112429	Morocco
NewSat-31	Mark IV	20230630_205114	New Mexico
NewSat-50	Mark V	20240918_175907	New Mexico
NewSat-48	Mark V	20240923_180612	New Mexico
NewSat-50	Mark V	20240923_180910	New Mexico
NewSat-50	Mark V	20241105_180508	New Mexico
NewSat-32	Mark IV	20240429_083727	Sicily
NewSat-26	Mark V	20240505_102252	Sicily
NewSat-43	Mark V	20240522_125040	Sicily
NewSat-48	Mark V	20240906_101044	Sicily
NewSat-50	Mark V	20240930_095029	Sicily
NewSat-34	Mark V	20230514_023539	Singapore
NewSat-27	Mark IV	20230605_035710	Singapore
NewSat-36	Mark V	20240803_034023	Singapore
NewSat-50	Mark V	20241111_034238	Singapore
NewSat-32	Mark IV	20241216_023013	Singapore

Table A3. Sensor spatial response parameters for 6 of 16 sensors. Sensors NewSat-27 and NewSat-31 are Mark IV generation, all others Mark V.

Sensor	Pixel Size (m)	Band	FWHM (pix)	MTF @ NF	FWHM (pix)	MTF @ NF
			Column Direction		Row Direction	
NewSat-27 Mark IV	1	NIR	2.21	0.020	2.22	0.020
		R	1.53	0.120	1.52	0.130
		G	1.07	0.290	1.12	0.270
		B	0.98	0.350	1.00	0.340
NewSat-31 Mark IV	1	NIR	2.08	0.040	2.10	0.040
		R	1.28	0.100	1.30	0.100
		G	1.13	0.230	1.12	0.270
		B	1.11	0.260	1.11	0.270
NewSat-41 Mark V	0.7	NIR	2.93	0.001	3.01	0.001
		R	2.61	0.008	2.75	0.007
		G	2.45	0.013	2.50	0.012
		B	2.39	0.014	2.40	0.014
NewSat-43 Mark V	0.7	NIR	3.98	0.000	4.00	0.000
		R	3.67	0.004	3.74	0.001
		G	3.55	0.004	3.63	0.002
		B	3.38	0.003	3.45	0.003
NewSat-48 Mark V	0.7	NIR	3.05	0.001	3.25	0.001
		R	2.70	0.003	3.04	0.001
		G	2.57	0.016	2.75	0.004
		B	2.40	0.015	2.90	0.002
NewSat-50 Mark V	0.7	NIR	3.29	0.002	3.21	0.002
		R	2.95	0.001	3.00	0.001
		G	2.71	0.005	2.64	0.007
		B	2.48	0.018	2.71	0.006

Table A4. Relative geolocation accuracy assessment results of images from Mark IV generation sensors. Highlights indicate locations with CE90 larger than the specification of CE90 < 10 m.

Site Name	# of Images	# of Valid Matches	X Offset (m)	Y Offset (m)	X StdDev (m)	Y StdDev (m)	X RMSE (m)	Y RMSE (m)	CE90 (m)	CE90-demean (m)
Mark IV										
Argentina	5	574	2.4	0.1	3.0	4.1	3.8	4.1	9.4	9.0
Morocco	8	2680	8.9	16.3	4.0	5.9	9.8	17.4	25.3	8.6
New Mexico	1	891	2.1	-10.2	4.5	3.7	5.0	10.8	16.1	N/A
Sicily	1	568	-2.2	11.3	3.4	4.5	4.0	12.2	17.4	N/A
Singapore	4	426	0.7	-6.6	5.4	7.8	5.5	10.2	18.9	15.3
Overall Summary	**19**	**5139**	**2.38**	**2.18**	**4.06**	**5.2**	**5.62**	**10.94**	**17.42**	**9.74**

Table A5. Relative geolocation accuracy assessment results of images from Mark V generation sensors. Highlights indicate locations with CE90 larger than the specification of CE90 < 10 m.

Site Name	# of Images	# of Valid Matches	X Offset (m)	Y Offset (m)	X StdDev (m)	Y StdDev (m)	X RMSE (m)	Y RMSE (m)	CE90 (m)	CE90-demean (m)
Mark V Generation										
Morocco	2	688	11.7	10.0	2.7	3.8	12.0	10.7	20.6	6.7
New Mexico	4	1891	1.4	5.6	2.7	4.1	3.0	6.9	10.8	6.6
Sicily	4	846	-5.7	9.1	3.7	3.7	6.8	9.8	16.1	7.4
Singapore	1	68	0.7	-4.4	3.6	9.6	3.6	10.5	20.4	N/A
Overall Summary	**11**	**3493**	**2.0**	**3.7**	**3.2**	**5.3**	**6.4**	**9.5**	**17.0**	**9.3**